Science of the Total Environment 748 (2020) 141226

Contents lists available at ScienceDirect

Science of the Total Environment

journal homepage: www.elsevier.com/locate/scitotenv

How tropical cyclone flooding caused erosion and dispersal of mercury-contaminated sediment in an urban estuary: The impact of Hurricane Harvey on Buffalo Bayou and the San Jacinto Estuary, Galveston Bay, USA

Timothy M. Dellapenna [a,b,*], Christena Hoelscher [a,b], Lisa Hill [b], Mohammad E. Al Mukaimi [c], Anthony Knap [a,d]

[a] Department of Oceanography, Texas A&M University, 3146 TAMU, College Station, TX 77843, USA
[b] Department of Marine Sciences, Texas A&M University-Galveston Campus, 1001 Texas Clipper Road, Galveston, TX 77554, USA
[c] Department of Marine Science, Kuwait University, Marine Science Center, Al Fintas Safat 13060, Kuwait
[d] Geochemical and Environmental Research Group (GERG), Texas A&M University, 833 Graham Road, College Station, TX 77845, USA

HIGHLIGHTS

- Hurricane Harvey caused massive flooding of the San Jacinto Estuary (SJE).
- Harvey eroded/deposited 16.4 × 106/ 7.73 × 106 tons of sediment from SJE.
- Eroded sediment sourced at least 2/3.9 tons of Hg from SJE/Buffalo Bayou.
- Main source of Hg is an industrial waste-water outfall in Patrick Bayou.
- The Harvey deposit in the SJE contains ~1 ton of Hg sourced from Buffalo Bayou.

GRAPHICAL ABSTRACT

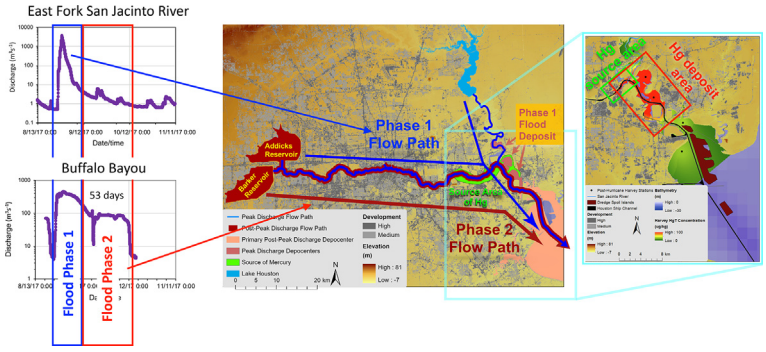

ARTICLE INFO

Article history:
Received 23 April 2020
Received in revised form 21 July 2020
Accepted 23 July 2020
Available online 31 July 2020

Editor: Damia Barcelo

Keywords:
Hurricane Harvey
Galveston Bay
San Jacinto River
Mercury
Flood deposit
Legacy contaminants

ABSTRACT

Hurricane Harvey (Harvey), a slow-moving storm, struck the Texas coast as a category 4 hurricane. Over the course of 53 days, the floodwaters of Harvey delivered 14×10^9 m^3 of freshwater to Galveston Bay. This resulted in record flooding of Houston bayous and waterways, all of which drained into the San Jacinto Estuary (SJE,) with its main tributaries being Buffalo Bayou and the San Jacinto River. The lower SJE and lower Buffalo Bayou has experienced up to 3 m of land subsidence in the past 100 years and, as a result, prior to Hurricane Harvey, up to 2 m of sediment within the upper seabed contained an archive of high concentrations of Total Hg (HgT) and other particle-bound and porewater contaminants. Within the SJE, Harvey eroded at least 48 cm of the sediment column, resulting in the transport of an estimated 16.4×10^6 tons of sediment and at least 2 tons of Hg into Galveston Bay. This eroded sediment was replaced by a Harvey storm deposit of 7.73×10^6 tons of sediment and 0.96 tons within the SJE, mostly sourced from Buffalo Bayou. Considering that the frequency of slow-moving tropical cyclones capable of delivering devastating rainfall may be increasing, then one can expect that delivery of Hg and other contaminants from the archived sediment within urbanized estuaries will increase and that what happened during Harvey is a harbinger of what is to come.

Abbreviations: BB, Buffalo Bayou; HgT, Total Mercury; SJE, San Jacinto Estuary; ng g^{-1}, nanograms per gram.

* Corresponding author at: Department of Oceanography, Texas A&M University, 3146 TAMU, College Station, TX 77843, USA.
E-mail addresses: dellapet@tamug.edu (T.M. Dellapenna), tknap@geos.tamu.edu (A. Knap).

https://doi.org/10.1016/j.scitotenv.2020.141226

1. Introduction

Many of the world's urbanized estuaries and deltas are experiencing elevated rates of subsidence (Jelgersma, 1996; Syvitski et al., 2009; Tessler et al., 2015; Al Mukaimi et al., 2018a), which can lead to the archiving of legacy contaminants in their sediments (Uncles et al., 1988; Olsen et al., 1993; Kennish, 2002; Swales et al., 2002;). If these legacy contaminants are buried by a few decimeters of sediment, they are generally believed to be buried deep enough with the seabed to no longer be susceptible to erosion (e.g. Cutshall et al., 1981; Olsen et al., 1993). However, these legacy contaminants can also be "environmental time bombs" if they do get eroded because they will then also be re-introduced to the water column where they can be broadly dispersed and detrimentally impact ecosystems and the environment. Numerous published studies have addressed the erosion of legacy contaminants within drainage basins, flood plains and river beds (e.g. Macklin et al., 1997; Turner et al., 2008; Ciszewski and Grygar, 2016) as well as within coastal landfills (O'Shea et al., 2018) and coastal mining sites (Ayuso et al., 2013). In addition, there are also numerous studies addressing the re-distribution of contaminated surficial sediments within estuaries (e.g. Cave et al., 2005; Schoellhamer et al., 2007; de Souza Machado et al., 2016; Rodriguez-Iruretagoiena et al., 2016), and the public health risk this exposure plays (Bera et al., 2019; Knap and Rusyn, 2016; Plumlee et al., 2013), however, there is a paucity of studies addressing the erosion of more deeply buried (i.e., deeper than a decimeter or more) legacy contaminants within an estuary, despite their potential existence within rapidly subsiding estuaries. This study adds to our understanding of how large storms and intense flooding within heavily industrialized and urbanized estuaries can erode nearly 0.5 cm of the bay bottom, and re-introduce and disperse tons of legacy Hg into surface sediments and the water column. Here, we assess the impact of unprecedented flooding due to Hurricane Harvey on the upper reaches of Galveston Bay, within Buffalo Bayou and the San Jacinto Estuary where there is a well-documented inventory of legacy contaminants buried down to depths greater than 50 cm (Al Mukaimi et al., 2018a).

Buffalo Bayou flows 75 km, from the Barker and Addicks reservoirs through the heart of metropolitan Houston and empties into the SJE, which then flows into Galveston Bay (Fig. 1). Houston is the fifth-largest metropolitan area in the United States, (population of 7 million) and is the fourth-largest city in the US. Houston hosts the second-largest petrochemical complex in the US and second in the world (Morse et al., 1993; Santschi et al., 2001). The Port of Houston is the second-largest seaport in the U.S. in terms of total shipping tonnage (Chambers et al., 2018). Galveston Bay and the SJE are micro-tidal, with a tidal 0.5–0.7 m tidal range (Armstrong, 1982; Solis and Powell, 1999). The bay is considered to be meteorologically dominated, given its small tides, shallow depths, and high susceptibility to wind forces (Solis and

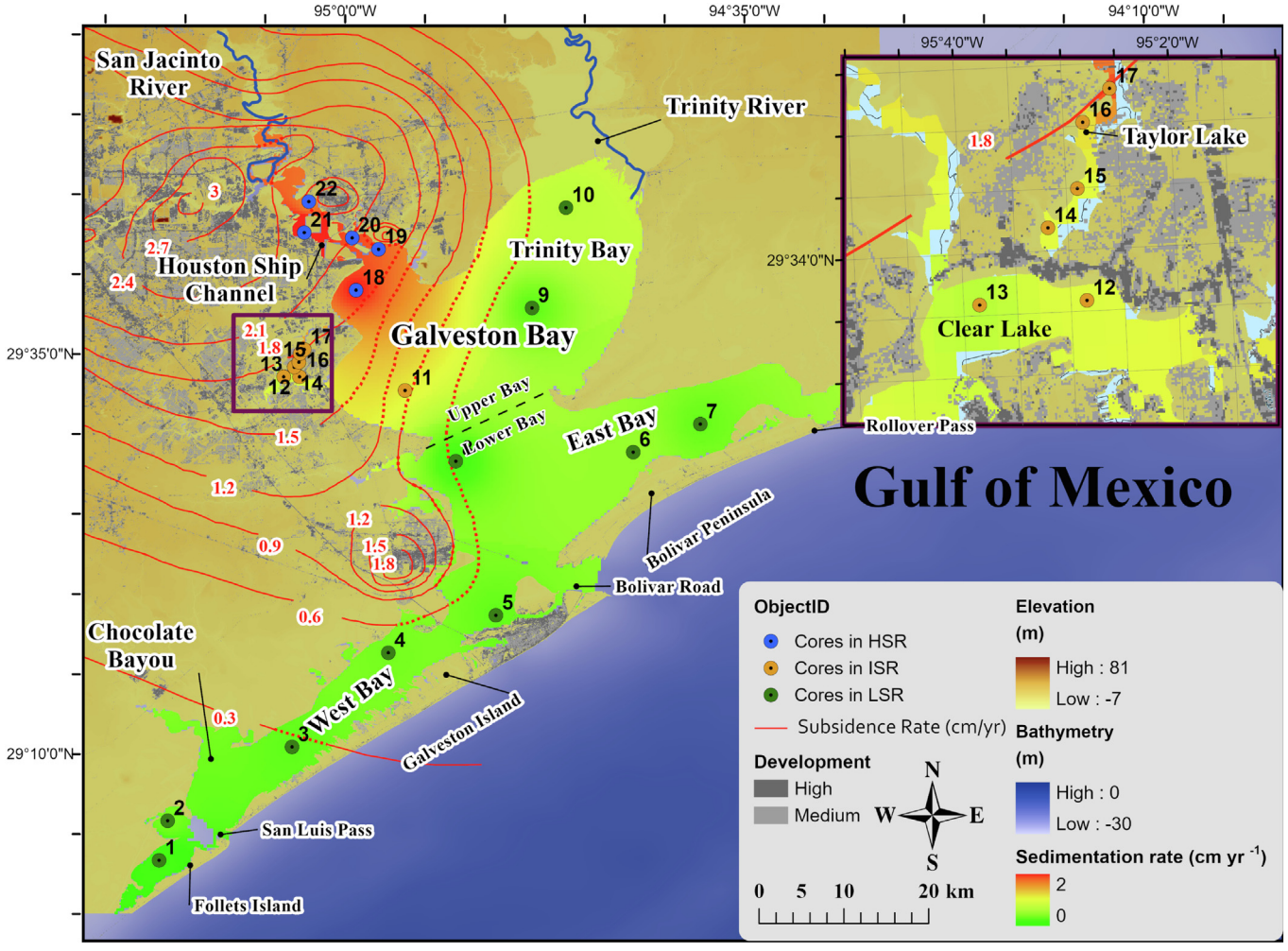

Fig. 1. Galveston Bay subsidence and sedimentation rate map contour plot (red line) of subsidence (meters) between 1906 and 2000 (HGSD, 2008). The gray shaded area represents the Trinity River incised valley (Rodriguez et al., 2005). Note, the highest subsidence was within the San Jacinto Estuary and Buffalo, with subsidence of 2.5–3.0 m (~3 cm y^{-1}) and sedimentation rates averaging 2 cm y^{-1} indicating that although there were extremely elevated sedimentation rates, sedimentation did not keep pace with subsidence (from Al Mukaimi et al., 2018a).

Powell, 1999; Ward, 1980), with cold fronts driving much of the sediment resuspension and transport (Carlin et al., 2016).

Elevated groundwater was withdrawn to both support the expanding population of metropolitan Houston as well as the growing petrochemical complex. This has resulted in elevated land subsidence across much of both greater Houston and also upper Galveston Bay (Fig. 2), with as much as 3 m of subsidence since 1900 focus the area of lower Buffalo Bayou, the San Jacinto Estuary (SJE) and upper Galveston Bay, as the Houston Petrochemical complex (Coplin and Galloway, 1999; HGSD, 2013). Al Mukaimi et al. (2018a) addressed the question of whether sedimentation kept pace with subsidence and found that within the lower SJE, where subsidence rates averaged 3 cm yr^{-1}, sedimentation was at half of this rate, averaging 1.5 cm yr^{-1}. Al Mukaimi et al. (2018b) found that the elevated subsidence within the lower SJE resulted in the elevated preservation of legacy contaminants, including Hg, Pb, Ni, and Zn. In sediment core C-22, a peak in HgT of 2374 ng g^{-1} was found at 77 cm within the core and elevated HgT concentrations were found as deep as 110 cm (Fig. 3) with background concentrations of HgT between 20 and 50 ng g^{-1} throughout Galveston Bay.

Mercury (Hg) is one of the most detrimental global aquatic contaminants (Bank, 2012; Liu et al., 2011). In marine environments, Hg bioaccumulates as methyl mercury, contaminates seafood, and thus poses a human health hazard (Di Leonardo et al., 2006). There are likely numerous sources of Hg within the Galveston Bay drainage basin, including atmospheric outfall from coal combustion, effluent from wastewater treatment, agricultural runoff, and various industrial runoffs (Al Mukaimi et al., 2018b). However, historically, the greatest, and likely the dominant source of Hg within the drainage basin appears to be industrial wastewater runoff from Patrick Bayou (PB), a small tributary of Buffalo Bayou, with a water surface area of 0.18 km^2, located 4 km upstream from the confluence of Buffalo Bayou and the SJE. Patrick Bayou is a US Environmental Protection Agency (EPA) Superfund Site for Polyaromatic Hydrocarbons (PAHs), Polychlorinated Biphenyls (PCBs), Dioxins, Hg, and several other industrial contaminants (US EPA, 2017). Industrial wastewater discharge into PB from a Chloralkali plant located within Patrick Bayou is listed by the EPA as the likely source of the contamination (US EPA, 2017). The Texas Natural Resources Conservation Commission (TNRCC) reported that during a site inspection in 2000, sediment samples collected in PB had HgT levels as high as 41,500 ng g^{-1}. Patrick Bayou is located in an area that has experienced over 3 m of subsidence. A summary of a report from the US EPA was found online (HGAC, 2012) showing results of a sediment core collected upstream of the bridge in PB, directly in front of the outfall. A profile of HgT shows peak HgT concentration at ~130 cm depth and peak PCB's at 100 cm, indicating over 1.5 m of archived legacy contamination within Patrick Bayou.

Al Mukaimi et al. (2018a) investigating the historical input of Total Mercury (HgT) into Galveston Bay (Fig. 4A). In this study, they found that surface HgT concentrations vary widely from site to site, ranging from between 6 and 162 ng g^{-1}, with an average of 50.0 ng g^{-1}, generally following the previously reported range of 10–280 ng g^{-1} (Morse et al., 1993; Santschi et al., 2001). Al Mukaimi et al. (2018b) also

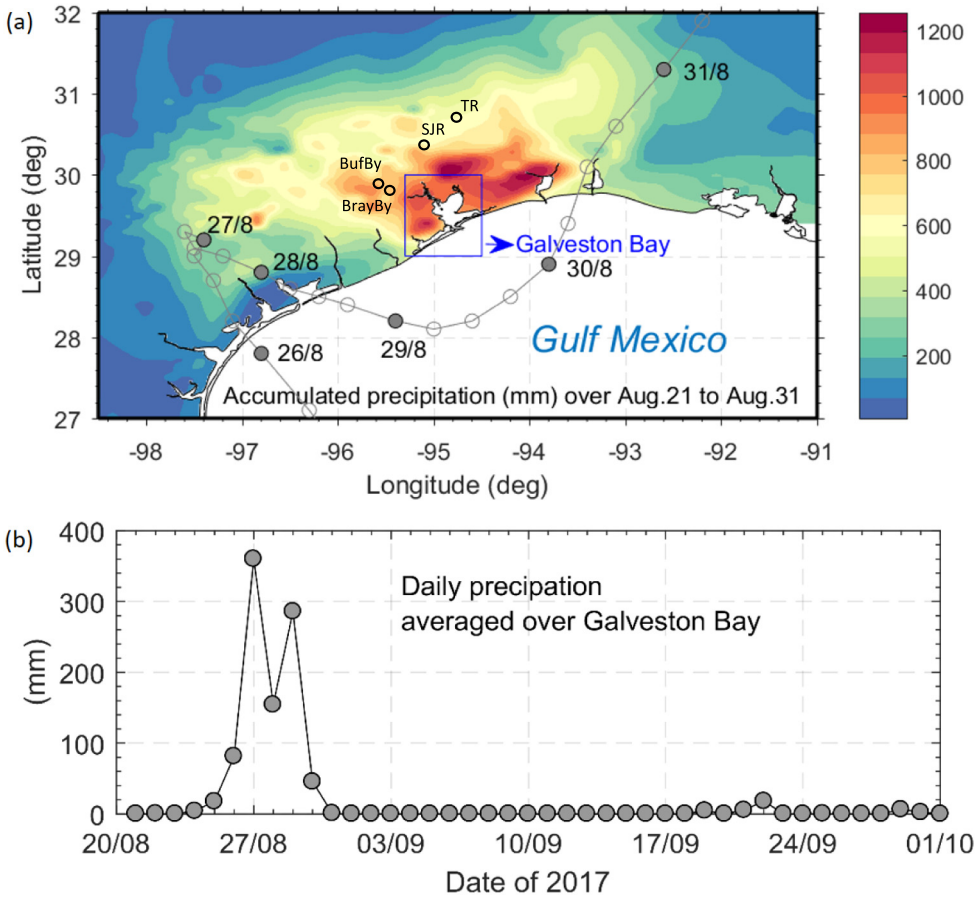

Fig. 2. Hurricane Harvey Rainfall for Metropolitan Houston and eastern Texas. (a) Accumulated precipitation during Hurricane Harvey between August 21 and 31, 2017 and (b) daily precipitation averaged over Galveston Bay (30 weather stations). In (a), the 6-hourly track (all times in UTC) of Hurricane Harvey, based on data from National Hurricane Center (https://www.nhc.noaa.gov), is shown with circles. Precipitation data in (b) are based on daily records extracted from the Global Historical Climatology Network (https://www.ncdc.noaa.gov) (after Du et al., 2019a).

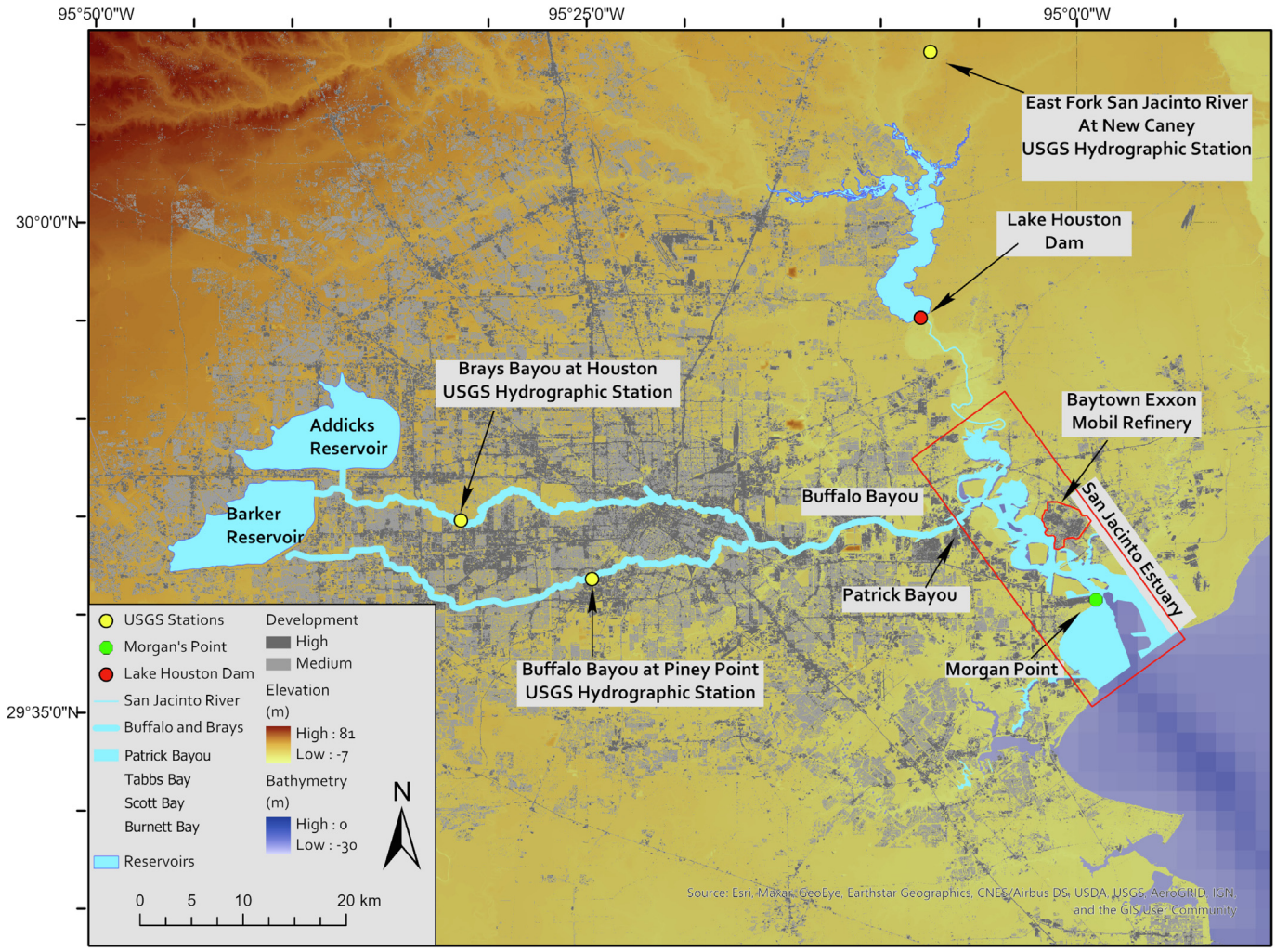

Fig. 3. Base map of the study area. Base map showing the location of the Addicks and Barker Reservoirs as well as the location of Buffalo Bayou, Patrick Bayou, and the San Jacinto Estuary.

documented background concentrations of HgT, in deeper sections of the core (Fig. 5A), likely deposited during the pre-Industrial period of the bay, ranged range from 8 to 20 ng g^{-1}. NOAA considers levels of 4–51 ng g^{-1} as background conditions (Buchman, 2008).

Hurricane Harvey (Harvey) struck the Texas coast between 25 and 27 August 2017, making landfall as a category 4 hurricane, and delivering between 76.2 and 127 cm of rain to the Houston Metropolitan area and the drainage basin of Galveston Bay (Fig. 2; NOAA, 2017). Over the course of 44 days, the floodwaters of Harvey delivered 14×10^9 m^3 of freshwater to Galveston Bay, a volume equivalent to 3.7 times the volume of the entire bay (Du et al., 2019a, 2019b). This record rainfall resulted in unprecedented flooding of Houston bayous and waterways, all of which drained into the SJE, with its main tributaries being Buffalo Bayou and the San Jacinto River. The associated river discharge delivered 149×10^6 tons of sediment to the bay, which constitutes 35 yrs. of normal fluvial sediment yield (Du et al., 2019a, 2019b).

Harvey was a slow-moving tropical cyclone. The amount of precipitation a tropical cyclone delivers is inversely proportional to the translational speed of the storm (Kossin, 2018), thus, slower-moving storms deliver more precipitation than fast-moving storms, having the potential to deliver substantially greater volumes of floodwaters. Since 1949, globally, there has been a 10% decrease in the translation speed of storms (Kossin, 2018). With an increase in anthropogenically enhanced climate change, there is also a trend towards an increase in persistent weather extremes (Mann et al., 2017), an increase in the frequency and intensity of tropical cyclones (Held and Soden, 2006; He and Soden, 2015; Vecchi and Soden, 2007; Vecchi et al., 2006, and He et al., 2017), and, with an increase in global temperature, there is also an anticipated increase in the amount of rain associated with tropical cyclones (Kossin, 2018; Walsh et al., 2016). These slow-moving storms can cause catastrophic flooding, as was the case with Harvey (2017) and more recently Hurricane Florence (2018), which struck Wilmington, NC. When this intense precipitation falls within the watersheds of urbanized/industrialized estuaries, the associated floods increase the risk of erosion and dispersal of legacy contaminated sediments (e.g. Santschi et al., 2001). If the urbanized/industrialized estuary has been subjected to elevated subsidence rates, then there is an even greater likelihood that sediments within the urban river/estuary contain an archive of elevated levels of legacy contaminants, which are potentially available for erosion and dispersal. The impact of Harvey provides the opportunity to investigate what happens when a heavily industrialized estuary, which has undergone significant land subsidence and which sediment contains an archived of legacy contaminants, is hit by a major flood event associated with a slow-moving hurricane. This paper reports on how the flooding associated with Harvey eroded and transported massive amounts of mercury contaminated sediment within Buffalo Bayou, Patrick Bayou, and the SJE. To address this question, results from vibra-cores collected and analyzed pre-Harvey are compared to results from vibra-cores and push cores collected post-Harvey within the SJE and the collection of vibra-cores in Patrick Bayou, a tributary of lower Buffalo Bayou.

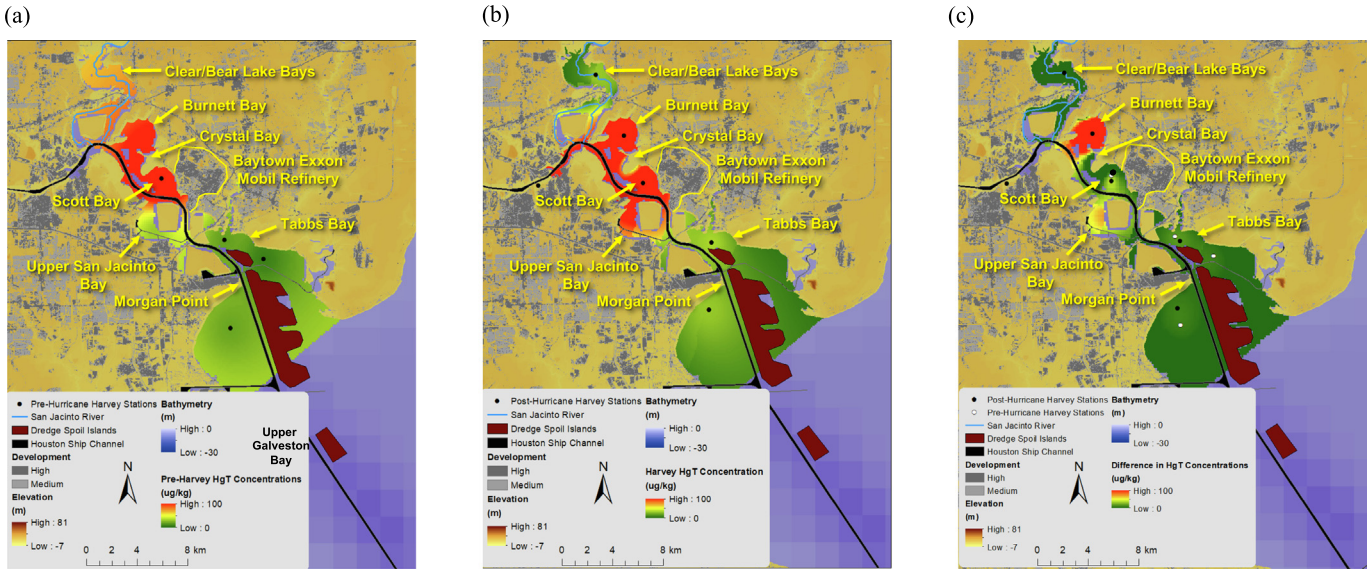

Fig. 4. Surface Sediment Total-Hg (HgT) maps for the San Jacinto Estuary (SJE). A) The pre-Harvey HgT Concentrations map for surface sediment is from Al Mukaimi et al. (2018a) and shows that the highest concentration of HgT is centered around Burnett and Scott Bay, Buffalo Bayou was not sampled pre-Harvey. B) Post Harvey HgT shows again that the highest concentrations are in Burnett and Scott Bay. Note, the map scale only goes up to 100 ng g^{-1}, but the surface sediment in Burnett and Scott Bays have HgT concentration of 670 and 195, ng g^{-1}, respectively. C) shows the HgT Difference maps and shows that the greatest enrichment of HgT was in Burnett Bay and the enrichment becomes progressively southward towards Galveston Bay. HgT is depleted in the Harvey deposit northward upstream of the confluence of Buffalo Bayou and the SJE, indicating that the source of HgT was from Buffalo Bayou and not the San Jacinto River.

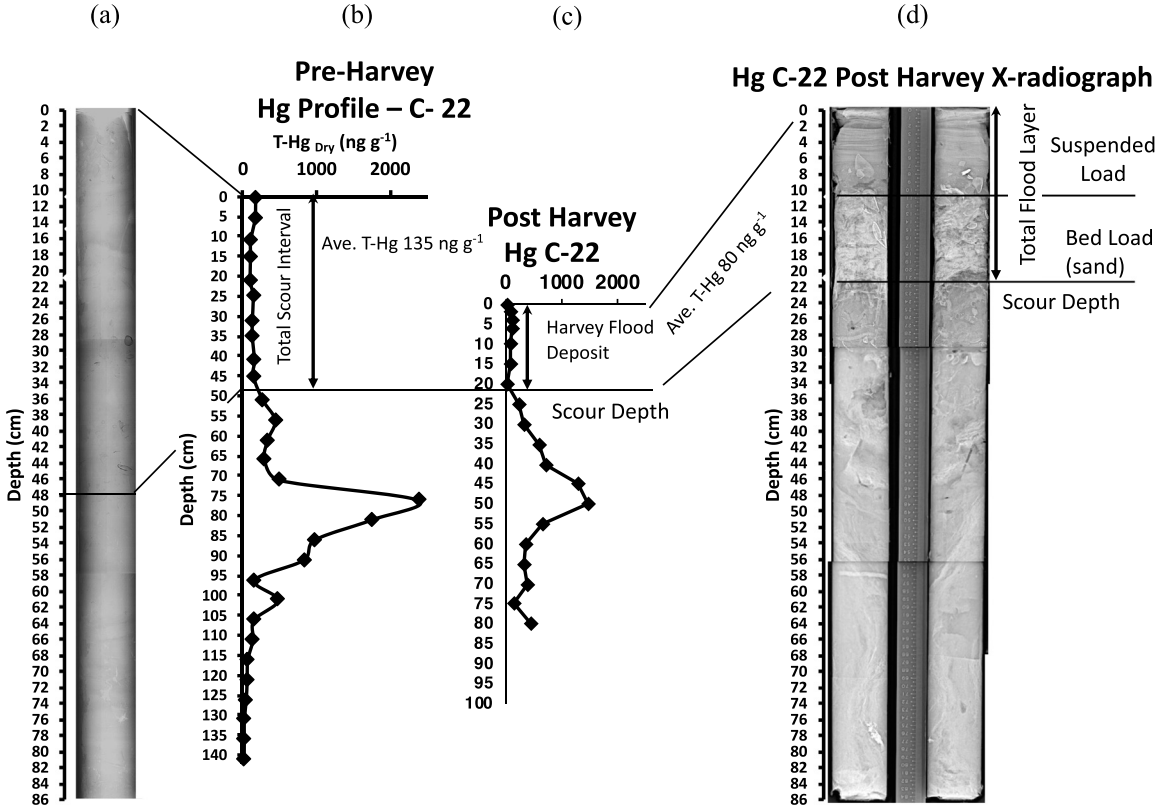

Fig. 5. Comparison of pre- and post-Hurricane Harvey core C-22 from Scott Bay. (a) Pre-Harvey Total Hg (HgT) sediment profile and (b) post-Harvey HgT sediment profile, both from Al Mukaimi et al. (2018a). (c) Hg profile and (d) x-radiograph from post-Harvey C-22. The peak HgT was used to correlate between cores. When comparing the pre-Harvey (a) and post-Harvey (c) HgT profile and x-radiographs (b) and (c), it is revealed that 48 cm of sediment was eroded. The post-Harvey x-radiograph (d) reveals an erosional surface, above which sits a shell and sand layer, which represents the flood bedload deposit. Above this, a mud dominated layer representing the suspended load deposit. Note an increase in average HgT in the Harvey deposit of 197 ng g^{-1} when compared to the pre-Harvey HgT of 80 ng g^{-1}.

2. Material and methods

2.1. Data collection and core processing

Core 22 and Patrick Bayou Core 1 were collected as vibra-cores using a 7.6 cm diameter aluminum barrels. The vibra-cores were collected using an Oztec vibra-coring head attached to a 7.6 cm diameter aluminum barrel, with core recovery ranging from 1 to 4 m. The cores were brought back to the lab, split axially, using power shears to cut the core barrel and wire used to cut the core. One half of the core was subsampled, with half of the core preserved under refrigeration for archival purposes. Core 22 was collected in August of 2012, and analyses of Core 22 are reported in Al Mukaimi et al. (2018a, 2018b). Patrick Bayou Core 1 was collected on May 8, 2019.

Push cores were collected using a repurposed Benthos® checkvalve pushcoring head, which was attached to an aluminum conduit with stainless steel hose-clamps and electrical tape. The conduit was in 1.5 m long sections that screwed together, with a maximum length of 5 m. The removable core barrels consist of 7.6 cm diameter polycarbonate tubes generally ranging in length from 0.3 to 0.6 m. During recovery, the pushcoring system was brought to the surface and the core barrels were capped while the end of the core was still in the water to prevent the loss of the cores from the check valve. While holding the core vertically, the bottom core cap was immediately sealed with electrical tape while still being kept vertical. Flourofoam was pushed into the core top so that it rested just above the sediment-water interface, the flourofoam was cut flush with the top of the core barrel and then the top of the core was sealed with a core cap and electrical tape and stored vertically for transport back to the lab.

None of the recovered cores showed any signs of degradation from transportation. The cores were stored in a cold room which is held at a constant temperature of 4 °C. X-radiographs were taken of all cores at an energy level of 64 kV and exposure time of 1.6 mAS with a portable Medison X-ray source and a Varian PaxScan® Amorphous Silicon Digital Imager.

After each core was x-rayed, the entire Harvey layer was extruded. In some cases, each one-centimeter interval was collected, in others, the entire interval was extruded as a single sample. For those for which the sediment was extruded into 1 cm intervals, a subsample of each interval of equivalent volume was combined to make a single Harvey sample and homogenized and subsamples of this were collected for Hg and grain size analyses. For those samples where the entire interval was sampled, the interval was homogenized and subsamples were collected for Hg, grain size distributions, and water content.

2.2. Water content and porosity

Samples (10 g) collected when the cores were sampled and were immediately placed in pre-weighed aluminum tins and kept in an oven at 50 °C for at least 24 h, and then re-weighed to determine water content. The porosity was calculated from the water content by estimating the salt content, using an average sediment density of 2.65 g cm^{-3}.

2.3. Total Mercury analysis

For the analysis of total mercury concentration (HgT) in the sediments, approximately 100 mg of dry and homogenized pulverized sediment samples at 5 cm intervals were analyzed using Direct Mercury Analyzer (DMA-80, Milestone SRL, Italy) which is compliant with U. S. EPA Method 7473 (EPA, 1998). The DMA-80 was calibrated using prepared standard solutions of mercury and the calibration curve was verified with Certified Reference Materials (CRM). In order to ensure precision, reliability, accuracy, and consistency of the sediment samples for the total Hg, three CRMs (MESS-3 Marine sediment (0.091 ± 0.009 mg l^{-1}, National Research Council of Canada), NIST 2702 Inorganics in Marine sediment (0.4474 ± 0.0069 mg l^{-1}, National Institute of Standards and Technology), and PACS-2 Marine sediment (3.04 ± 0.2 mg l^{-1}, National Research Council of Canada)) were used representing a different Hg range. Once the instrument was calibrated with liquid standard solutions, the calibration curve was verified with the three CRMs. Blanks and duplicates were analyzed every 10 samples to ensure accuracy. The results obtained from the CRMs were excellent and in good agreement within the certified range with an average recovery rate for MESS-3 of 97% ± 7% (Mean ± RSD, n = 137), NIST 2702 (96% ± 7% (Mean ± RSD, n = 43), and PACS-2 (97% ± 11% (Mean ± RSD, n = 64).

2.4. Geographic Information System (GIS) map preparations and volume and mass calculations

The maps used in this study were created using various ArcMap Pro 2.5.1 mapping tools. The basemaps were created using elevation data from the United States Geological Survey and bathymetry data (USGS, 2013) from the Texas Parks and Wildlife Department (TPWD, 2013). The development data was retrieved from NOAA (NOAA, 2016). The raw data set was inserted into ArcGIS and was reclassified so that only medium to high development is shown. The shoreline data was retrieved from the Texas Natural Resources Information System (TNRIS, 2014). Contours of the data were generated using the Inverse Distance Weighted (IDW) tool, which assumes that the influence of a variable decreases with distance.

The flood deposit volume was determined based on the contoured data for each sub-bay and converted to mass by assuming a water content of 70% and a sediment density of 2.65 g cm^3, which is the density of quartz. To estimate HgT masses for each sub-bay, an average concentration was used for each sub-bay and the concentration was multiplied by the mass of sediment within the sub-bay.

3. Results

3.1. Comparisons of vibracores and pushcores in San Jacinto Estuary

Bear Lake and Clear Lake are represented by SJRVC-1, which was collected in Clear Lake, 6 river km upstream from the confluence of the San Jacinto River and Buffalo Bayou, and is the only core collected upstream in the SJE upstream of Buffalo Bayou. The Harvey layer in SJRVC-1 was 6.25 cm thick and had a HgT concentration of 30 ng g^{-1}. Burnett Bay had a Harvey thickness of 31.5 cm and a surface HgT concentration of 670 ng g^{-1}.

The pre and post-Harvey Cores 22 were collected at a site within Scott Bay, which is a small, semi-enclosed bay within the SJE in an area where the average Relative Sea Level Rise rate for the past century is estimated to be 2.78 5 cm y^{-1} (Al Mukaimi et al., 2018a). In 2012, pre-Core 22 was collected and subsequently analyzed by Al Mukaimi et al. (2018a, 2018b) for down core concentrations of Hg, x-radiographs were collected as unsplit core x-rays, down core grain size distributions and ^{210}Pb geochronology was performed on the core (Fig. 5). Based on these analyses, it was determined that the average sediment accumulation on this core was 1.5 cm y^{-1}.

In the pre-Harvey Core 22, the x-radiographs and the grain size profiles reveal that the core is consistently composed of 90–98% mud with only 2–10% sand. In pre-Harvey Core 22, there is a prominent Hg spike in concentration of 2374 ng g^{-1} at 76 cm, according to Al Mukaimi et al. (2018b), this corresponds to a depositional event estimated to have happened around 1972. Above this spike, the concentration of Hg sharply decreases and at the surface, the Hg concentration is 162 ng g^{-1}.

In Post-Harvey Core 22, the x-radiograph was taken from a split core and reveals the presence of a 22 cm thick layer at the surface of the core. The base of this new layer is marked by an erosional surface above which is a basal deposit 12 cm thick consisting of shell gravel and sand. The shell layer included intact shells up to 2–3 cm long and coarse

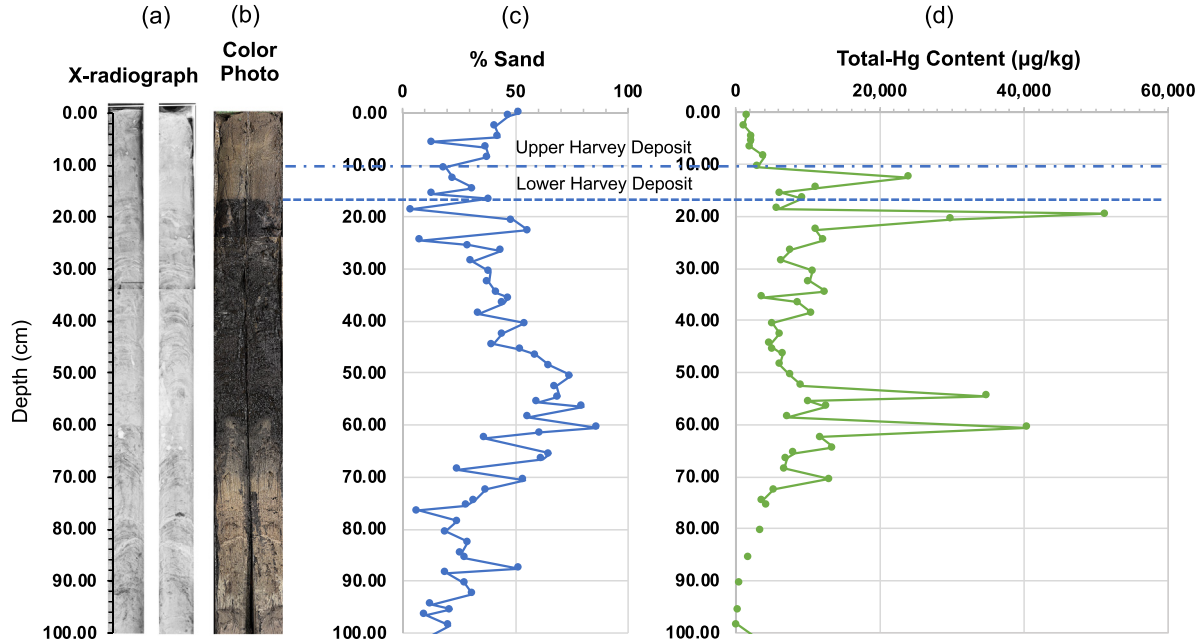

Fig. 6. (a) X-radiograph, (b) color photograph, (c) percent sand content, Total-Hg (HgT) content of Patrick Bayou Core 1. The color photograph (b) shows the Harvey layer as a brown, oxic layer, sitting atop a black, anoxic layer. The x-radiograph (a) reveals that the Harvey layer is generally featureless, suggesting rapid deposition. The percent sand content profile (c) and HgT (d) both reveal that there is a lower, mud dominated averaging 10,000 ng g^{-1}, whereas the upper Harvey layer is sand dominated and has a much lower HgT averaging 2255 ng g^{-1}.

shell fragments. There is a sharp transition at 10 cm in the core, above which there is a layer of well-laminated mud, with sandy laminations, the average sand content of this interval is 25%. This upper 22 cm thick layer found in post-Harvey Core 22 is interpreted as the Harvey layer, with the coarse, basal portion of the flood layer represents bedload transported during the higher flow conditions and the finer upper layer having been deposited during the waning phase of the flood and represents deposition of the suspended load.

The erosional surface within the x-radiograph at the base of the flood layer suggests that there was erosion of the bed during the peak flood discharge conditions. Comparisons of HgT profiles from pre- and post-Harvey Core 22 reveal that at depth, below the flood layer, the HgT profiles correlate well with the 1972 peak HgT spike at 51 cm in the post-Harvey core. The pre-Harvey core collected in 2012 and additional cores collected in 2016 (shown in Hill, 2020) at the Core 22 site all reveal comparable HgT profiles. While the pre-Harvey Core 22 contained no significant or discernable sand layers within the upper 1 m of the core (Al Mukaimi et al., 2018b), aligning the HgT spikes in both cores show that ~48 cm of mud was eroded at the post-Harvey site prior to deposition of the 22 cm thick flood layer. The average concentration of HgT within the muddy portion of the Harvey flood layer was 197 ng g^{-1}.

3.2. Patrick Bayou Core results

Patrick Bayou Core 1 (PBC-1) was collected on May 8, 2019. As noted above, all of the samples were wet sieved to remove sand prior to measuring HgT concentrations, so these concentrations are not significantly skewed due to grain size variabilities. Core photographs (Fig. 6A) reveal that the upper 17 cm of the core contains brown sandy mud and the x-radiograph revealed this layer to be the base of which is delineated by a sharp contact. The upper 17 cm interval appears to consist of two intervals, a basal layer from 10 to 17 cm and a surface layer from 0 to 10 cm. The basal layer has a sand content averaging 22% and it progressively increases upwards from 13.6% at 17 cm to 38% sand at 10 cm and has a HgT concentration averaging 10,762 ng g^{-1}, with a peak HgT concentration of 24,011 ng g^{-1} at 12.5 cm. The x-radiograph reveals no bedding horizons, although there does appear to be a horizontal fabric. In addition, there are a few vertical burrows, suggesting escape burrows and also other vertical sedimentary structures indicative of fluid escape structures, which extend all way to the surface of the core. The fluid escape structures suggest dewatering due to rapid sedimentation, consistent with a storm deposit. The interval from 0 to 10 cm has a higher average sand at 38% with the surface interval having a sand content of 52%, a HgT concentration ranging from 1243 to 4004 ng g^{-1}, with an average HgT of 2255 ng g^{-1}, and generally looks similar to the layer below. It is assumed that the layer from 0 to 17 cm represents the Harvey layer. Directly below the Harvey layer, the HgT concentration is 51,270 ng g^{-1}, the highest concentration found within the entire core, and below this, from 21.5 to 40 cm, the HgT concentrations are generally 10,000 ng g^{-1} or higher. Additionally, from 20 to 60 cm, the core contains black mud, which had a very strong petroleum smell when the core was split and within this interval, the sand content within the core progressively decreases upwards from 69% at 55 cm to 4.2% at 20 cm. The HgT concentration of 51,270 ng g^{-1} at 19.5 cm is over 1000 times background concentrations and is the highest concentration found anywhere else in Galveston Bay, by a factor of 20.

3.3. San Jacinto Estuary Pushcore Harvey layer thickness estimation results

Only the portions of the SJE outside of the dredged and navigable channel are considered in this study. A combination of extremely high vessel traffic, maintenance dredging, and water depths precluded sampling within the ship channels. A total of 6 sites within the SJE were cored to determine deposit thicknesses, each of these sites were within sheltered bays, including Scott, Tabbs, and Burnet Bays, as well as Bear Lake and the upper SJE.

From the x-radiographs, the base of the Harvey layer was determined as well as the thickness of the layer and recorded (Table 1). For each core, the base of the Harvey deposit was easily identified as an anomalous erosional surface with a sand layer sitting atop of it, and above this a high-water content mud deposit (Figs. 5D and 6A). The sand layer was clearly evident as a lighter tone in the x-rays and is an

Table 1
Hurricane Harvey sediment and HgT loads for San Jacinto Estuary and Patrick Bayou.

Sub-Bay	Sediment mass deposited	Mass of HgT deposited	Sediment mass scoured	Mass of HgT scoured
Burnet Bay	7.87×10^5 tons	0.70 tons	1.72×10^6 tons	1.15 tons
Scott/Crystal Bay	1.01×10^6 tons	0.20 tons	2.21×10^6 tons	0.43 tons
Tabbs Bay	3.18×10^6 tons	0.10 tons	8.49×10^6 tons	0.25 tons
Upper San Jacinto Bay	7.52×10^5 tons	0.04 tons	1.64×10^6 tons	0.08 tons
Clear/Bear Lake	1.74×10^6 tons[a]	0.05 tons[a]	2.39×10^6 tons[a]	0.07 tons[a]
Patrick Bayou[a]	2.43×10^4 tons[a]	0.24 tons[a]	1.43×10^5 tons[a]	1.43 tons[a]
Total for San Jacinto Estuary Sub Bays	7.73×10^6 tons	0.96 tons	16.42×10^6 tons	2.0 tons

[a] Not included in total for the San Jacinto Estuary.

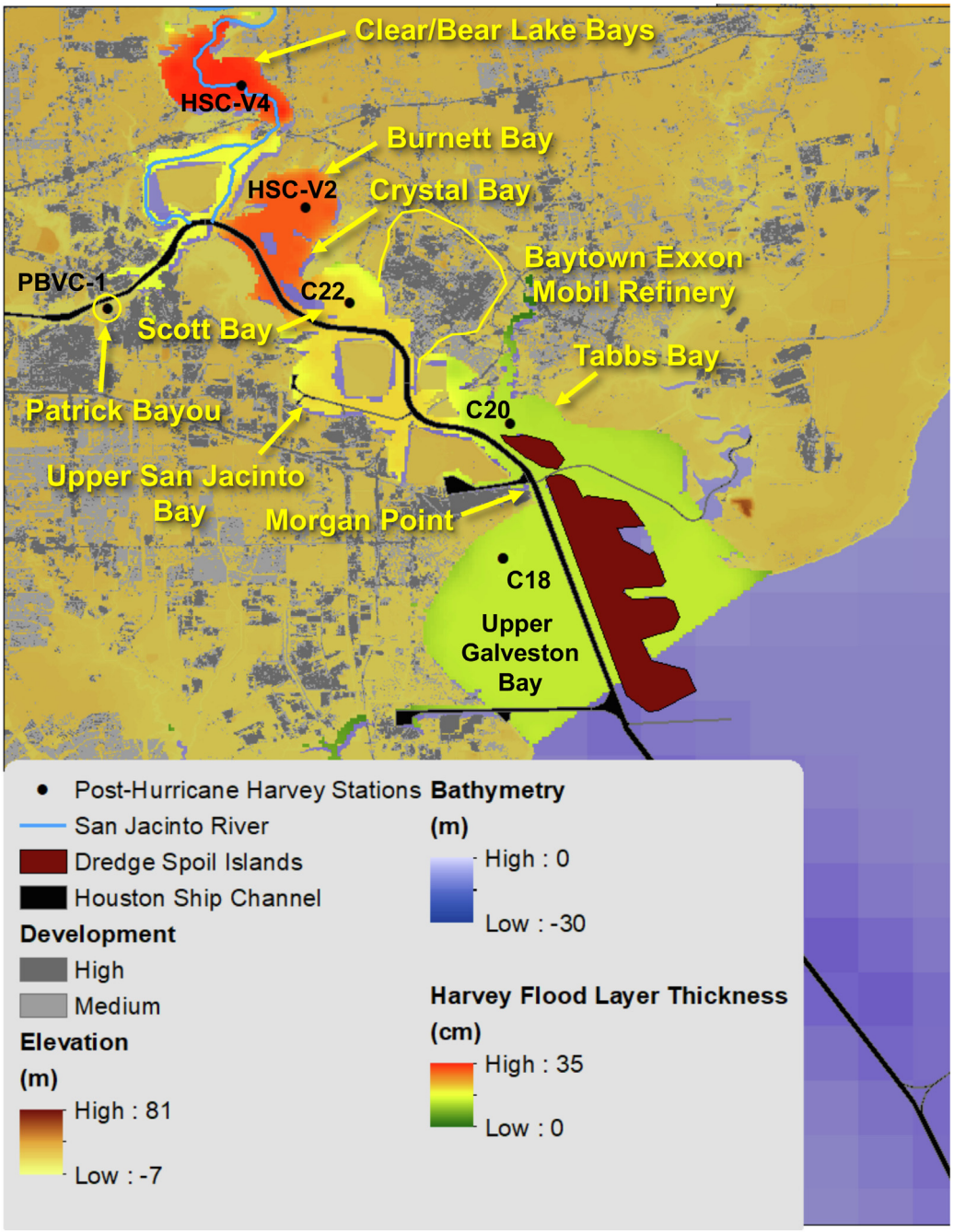

Fig. 7. Isopach map of Hurricane Harvey deposit in the San Jacinto Estuary. This map does not include the thickness of the Harvey deposit within the Houston Navigational Channel but extrapolates deposit thicknesses from the undredged areas across the navigation channel as a minimum thickness estimate. The thickest deposit was found in Core HSC VC-4, which is downstream from the Lake Houston Dam spillway. The next thickest deposit was found in Burnett Bay, where Buffalo Bayou flows into the San Jacinto Estuary. The deposit becomes progressively thinner towards the mouth of the San Jacinto Estuary within upper Galveston Bay.

anomalous feature within these cores as they were all collected in areas where the remainder of the cores are mud dominated. In most cores, there were also shells, many of which were articulated, also sitting atop the erosional surface.

Based on the measurements of the Harvey layer, an isopach map of the thickness of the Harvey deposit was generated for the portion of the SJE investigated, using ArcGIS (Fig. 7). Note, the contours on the map range from 0 to 50 cm, showing the range of cores from those areas outside of the dredged ship channel. For the basis of consideration of the Harvey deposit across the SJE, the dredged Houston Ship channel was ignored and the values from the adjacent areas are extrapolated across the channel areas as a minimum thickness estimate. The Harvey Isopach maps (Fig. 7) show that the thickest deposits were found within the SJE, south of the confluence with Buffalo Bayou, with thicknesses exceeding 50 cm in some places, and also forming a deltaic deposit in Galveston Bay at the mouth of the SJE.

Using ArcGIS, we determined the volume of the entire flood layer within the sub-bays of the SJE to be 9.72×10^6 m^3. Using the density of quartz (2.65 g cm^{-3}) for the sediment density and average water content for the flood deposit (70%), this volume of flood deposit contains a mass of 7.47×10^6 metric tons.

Within the SJE, the analyses of the Scott Bay core document 48 cm of sediment erosion within this bay. We have no other cores where we could effectively estimate the scour depth due to Harvey. However, the other portions of the SJE are generally less sheltered than Scott Bay, suggesting that comparable or greater currents were experienced in these locations. Assuming a scour depth of 48 cm and the same sediment parameters as assumed for estimating the mass of the Harvey deposit, with an area of the sub-bays of the SJE of 43 km^2, it is estimated that 16.4×10^6 tons of sediment was scoured from the SJE from Harvey and that this scoured sediment contained 2 tons of Hg (Table 1).

4. Discussion

4.1. Sources of Hg

According to Al Mukaimi et al. (2018b), Hg is sourced to Galveston Bay through both point-source and non-point sources. Non-point sources include atmospheric fallout from coal-burning and runoff from fertilizer, industrial waste streams from paper mills (e.g. Williams et al., 2015). However, there is one significant point source that has been identified, the wastewater outfalls of Patrick Bayou. Patrick Bayou (Fig. 8) is a 3 km long, sheltered slough that empties into lower Buffalo Bayou and contains seven industrial wastewater outfalls that empty into it. These include two outfalls from Oxyvinyl, (Occidental Chemical Company), as well as outfalls from Shell Oil Company and Lubrizol Corp. refineries. Hg has historically been used as a catalyst in the manufacturing of polyvinyl chloride (PVC; Vallette, 2018) and is a major source of Hg contamination throughout the world (e.g. Ren et al., 2014). PVC is one of the primary product streams of Oxyvinyl (Vallette, 2018).

Patrick Bayou was placed on the US EPA Superfund list for pesticides, polynuclear aromatic hydrocarbons (PAHs), and polychlorinated biphenyls (PCBs), after elevated levels of the contaminants were detected in its sediments in the early to mid-1990s (US EPA, 2017). Wastewater discharges from the outfalls within Patrick were attributed to be the primary sources of these contaminants. In addition, the Texas Natural Resources Conservation Commission (TNRCC), now called the Texas Commission on Environmental Quality (TCEQ), conducted samplings of Patrick Bayou in 2000 and found HgT levels as high as 41,500 ng g^{-1} as well as PCBs as high as 300,000 ng g^{-1} (US EPA, 2017). As noted above, core PB-C1 was collected on May 19, 2019. The two wastewater outfalls from the vinyl chloride processing plant are located 790 and 1100 m upstream for PB-C1. PBC-1 was collected approximately 200 m from the mouth of Patrick Bayou and ~50 m east of a low bridge that blocks vessel access to the remainder of the upstream portion of Patrick Bayou. The HgT from within the Harvey layer had an average concentration of 6122 ng g^{-1} and directly below the Harvey layer, the HgT concentrations were as high as 51,270 ng g^{-1}, indicating a that the core was collected proximal to the source of the Hg.

4.2. Hurricane Harvey Patrick and Buffalo Bayou flooding history and deposition

The Barker and Addicks Reservoirs are located ~75 river km to the west of the confluence of Buffalo Bayou and the SJE. Because of the retention of stormwater in the Barker and Addicks Reservoirs and the prolonged controlled release of these floodwaters, the Harvey flooding

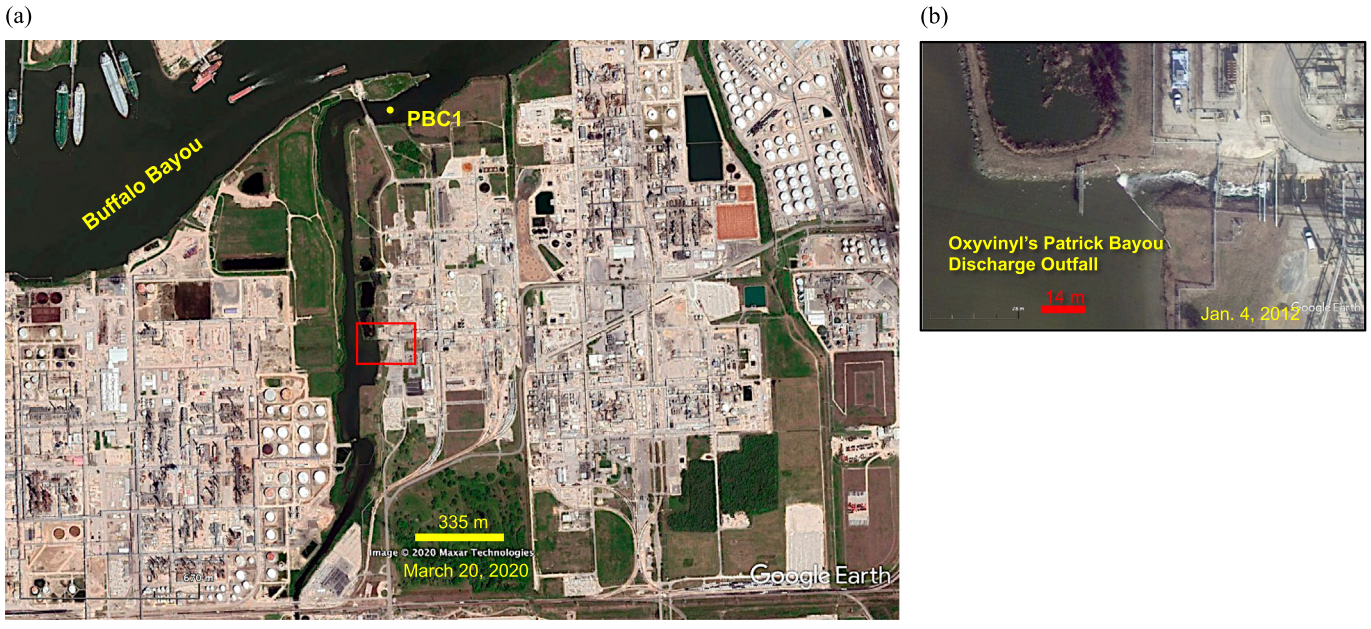

Fig. 8. Patrick Bayou map. A) Basemap from Google Earth March 20, 2020 of Patrick Bayou showing the location of the Oxyvinyl wastewater outfall in Patrick Bayou as well as the location of PBC-1 core location and its proximity to Buffalo Bayou. B) Map inset showing the Oxyvinyl wastewater outfall from the January 4, 2012 Google Earth image.

history of Buffalo Bayou is much different than the flooding histories of the other drainage basins within Galveston Bay. The flooding of Buffalo Bayou during Harvey can be divided into two phases, the first phase occurring during the peak discharge through the beginning of the release of floodwaters from the Barker and Addicks Reservoir. The second phase occurring during the extended-release of Addicks and Barker Reservoir flood water.

During the first phase of the flooding of the San Jacinto River, Brays Bayou, and the Trinity River, between August 23 to September 11, 2017, with peak discharges ending around September 5 or 6, depending on the river. For Buffalo Bayou, the peak discharge of $+200$ m^3 s^{-1} lasted for 16 days, from August 27 to September 11, 2017. Within Buffalo Bayou, the flood continued, settling down to a nearly continuous 80 m^3 s^{-1} during the controlled release, until it finally dropped off on October 13, 2017, for over an additional 32 days. Between Sept. 17 and Oct. 13, 2017, approximately 1.7×10^8 m^3 of floodwaters came from the Barker and Addicks Reservoirs.

During the period of time represented by the falling limb of the hydrographs, Aug. 28-Sept. 11 for the San Jacinto River/Estuary and Sept. 9–19, 2017 for Buffalo Bayou (Fig. 8), sediment deposition would have been occurring. For the SJE, as depicted in core Post-Harvey C-22 (Fig. 5C&D), the initial deposition is a basal deposit consisting of sand and gravel (shell), representing bedload. Above the basal bedload deposit is the upper layer, which is a mud dominated and represents the settling suspended load comprising the upper layer. However, because of the more complex history of the flooding in Buffalo Bayou, the deposit found in Patrick Bayou tells a different story. The 17 cm thick Harvey deposit in PB-C1 can be divided into two layers, a basal layer from 10 to 17 cm, which has a sand content averaging 22% and a HgT concentration averaging 10,762 ng g^{-1}, and a surface layer from 0 to 10 cm, which has an average sand content of 38% and an average HgT concentration of 2255 ng g^{-1}. The muddier basal portion of the Harvey layer in PB-C1 was deposited during the period representing the falling limb of the first flood pulse, prior to the opening of the Barker and Addicks Reservoirs. During this phase of the flood, Patrick Bayou and much of its drainage basin was flooded as well, and during the waning phase of this flood, higher Hg enriched sediment from the upper portion of Patrick Bayou was transported down the bayou and mixed with the Patrick Bayou drainage basin. The upper portion of Harvey flood layer appears to have been deposited during the period of time when the Barker and Addick Reservoir flood waters were released. During this phase of the flood, Buffalo Bayou waters and sediment would have flowed into Patrick Bayou, mixing with Patrick Bayou sediment. During this period, during the flooding of Buffalo Bayou, significant sand deposits were formed within the flood plain upstream of Patrick Bayou and the sediment load delivered during this phase of the flood would have had a significant sand component. The upper Harvey flood layer in the Patrick Bayou core generally has between 8 and 20% more sand than the lower layer and has a HgT averaging 20% of that found in the lower layer. With an average HgT of 2255 ng g^{-1}, it is still 4 to 10 times higher than what is found within the SJE Harvey deposit, suggesting significant mixing with Patrick Bayou derived sediment.

Based solely on the examination of our core, it is unclear whether there was significant erosion within Patrick Bayou during Harvey. However, there is a summary of a report from the Houston-Galveston Area Council (HGAC, 2012) showing results of a core collected upstream of the bridge in Patrick Bayou, directly in front of the outfall, showing a peak HgT concentration at ~130 cm depth. In PB-C1, the peak HgT is just below the base of the Harvey layer. If the sedimentation histories of these two sites are comparable, which seems reasonable, then this would suggest 130 cm of erosion from Patrick Bayou during Harvey. We found 48 cm erosion from within Scott Bay, which was much more sheltered than the PB-C1 site, so it is reasonable to assert that there was at least 1 m of erosion from Patrick Bayou. If we assume a thickness of 1 m, an area of 0.18 km^2, an average concentration of HgT of 10,000 ng g^{-1}, which is likely a conservative estimation, then the total mass of Hg within this one-meter thick layer of eroded sediment would have sourced 1.43 tons of Hg to Galveston Bay during Harvey. In addition, we estimate the HgT mass in the Harvey deposit to be 150 kg of HgT (Table 1), assuming that the flood layer has the same thickness as the PB-C1 core, of 17 cm thick and an average HgT concentration of 10,000 ng g^{-1}.

With the controlled releases from the Barker and Addicks Reservoirs, Buffalo Bayou flooded for 53 days, with a peak discharge (Fig. 9) at the Piney Point USGS Station of 424 m^3 s^{-1} and discharges of greater than 250 m^3 s^{-1} for 24 days, from Aug. 17 through Sept. 9. 2017. Pre-flood discharges were around 67 m^3 s^{-1}. The Morgan Point Tidal Gauge reported currents in excess of 2 m s^{-1} for five days, between August 27 and September 1, 2017, and in excess of 3 m s^{-1} for approximately 48 h within this interval (Du et al., 2019a). Much of the water flowing through Morgan Point would have been flowing through Buffalo Bayou and likely comparably high currents were flowing through Buffalo Bayou during this same period, with currents capable of significant erosion of the bed, which mainly consists of soft, easily erodible estuarine mud.

This discharge would have provided ample bottom shear stress to have significantly eroded the bed of Buffalo Bayou. According to the US Army Corps of Engineers, emergency dredging with the Houston Ship Channel above Morgan Point removed 8.8×10^5 m^3 of dredged material between Sept. 4–14, 2017 (pers. comm. with F. Fenner, USACOE), with significantly larger volumes dredged afterward.

4.3. Hg deposits in the San Jacinto Estuary

Analyses of the SJE is focused on the portion of the estuary from the north end of Bear Lake to the mouth of the estuary at Morgan Point, where it empties into Galveston Bay, and does not focus on the open ship channel areas of the estuary. The north end of Bear Lake is located 20 km downstream of the Lake Houston dam. Upstream of Bear Lake, the estuary is sand dominated and generally narrow, following the course of the San Jacinto River.

Core SJRVC-1, with a Harvey Layer thickness of 6.25 cm thick and a HgT concentration of 30 ng g^{-1}, is the only core collected above the confluence with Buffalo Bayou. The relatively thin Harvey thickness suggests that the sediment load delivered from the SJE was likely much lower than from Buffalo Bayou. The HgT concentration approaches background levels and considering the core was collected 6 km upstream of the confluence with Buffalo Bayou, it is reasonable to assume that very little Hg was transported to the lower SJE and Galveston Bay.

Core HSC-V2 was collected from Burnet Bay and the core location is 3.5 km downstream from the confluence of Buffalo Bayou and Patrick Bayou (Fig. 7). Core HSC-V2 had a Harvey layer 29 cm thick and has an average HgT concentration within the Harvey layer of 677 ng g^{-1}, the highest HgT concentration found within the Harvey layer outside of Patrick Bayou (Fig. 4B). The entrance to Burnet Bay is 2 km downstream from the confluence of Buffalo Bayou and the SJE, and is situated such that a significant volume of floodwater mainly from Buffalo Bayou would enter the bay during high discharge conditions but is configured such that the flow from the San Jacinto River would largely be blocked from entering Burnet Bay, so it would receive sediment primarily derived from Buffalo Bayou. In contrast, the location and configuration of Scott Bay (Fig. 7) is such that it likely received sediment both from the San Jacinto River as well as Buffalo Bayou. Analyses of Google Earth images from multiple flood events also show that there is less advection of turbid plumes derived from the San Jacinto River entering Burnet Bay when compared to Scott Bay. There were no pre-Harvey cores from Burnet Bay, so we have used the scour depth from Scott Bay to estimate the scour depth of Burnet Bay, although, given its location, this is likely an underestimation of the scour depth.

Core C-22 in Scott Bay, is located 5 km from the mouth of Buffalo Bayou and 9 km downstream of the mouth of Patrick Bayou. The average HgT concentration within the 22 cm thick Harvey layer in Scott

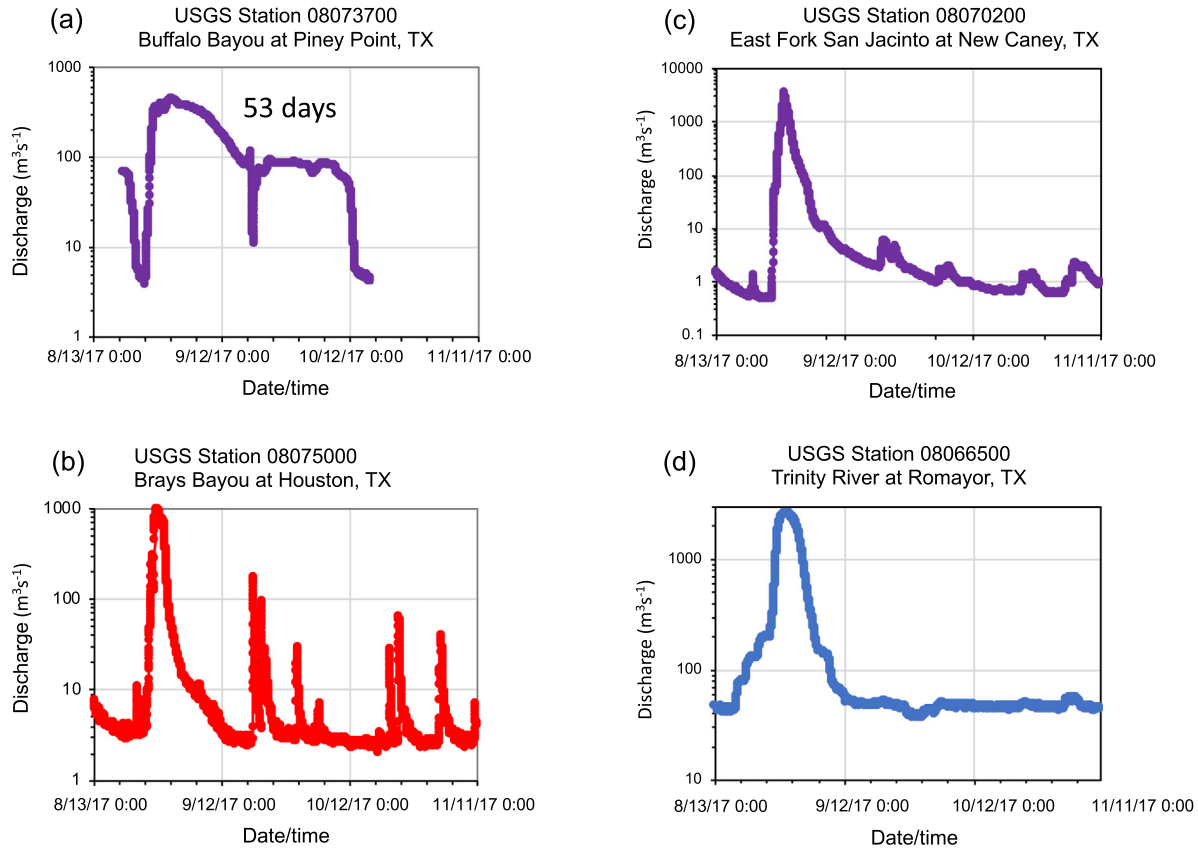

Fig. 9. USGS hydrographs from (a) Buffalo Bayou at Piney Point, (b) Brays Bayou, (c) East Fork of San Jacinto River, and (d) Trinity River at Romayor. Each of these rivers flows into Galveston Bay. Because of the controlled release of floodwaters from the Barker and Addicks Reservoirs (Fig. 3), Buffalo Bayou had two steps in the hydrograph (a), the first step, with higher discharge resulted from the initial phase of the flood, however, a prolonged, nearly flat section of the hydrograph at ~100 $m^3\ s^{-1}$ results from the prolong floodwater release, for a total of 53 days of flooding.

Bay is 197 ng g^{-1}. This lower HgT concentration suggests that the further from the source, the lower the HgT concentration, likely due in part because of the mixing of sediment from the San Jacinto River as well as Buffalo Bayou, diluting the high HgT enriched sediment derived from Buffalo Bayou with lower HgT concentration sediment derived from the San Jacinto River.

Downstream of Scott Bay, Upper San Jacinto Bay had only a 4.3 cm thick Harvey deposit. The Upper San Jacinto Bay is an open and exposed section of the river on the western side of the lower SJE (Fig. 7) and would have experienced the full current of the ebbing floodwaters from both the San Jacinto and Buffalo Bayou and had a HgT concentration of 48 ng g^{-1} (Fig. 4B), which is essentially background. Tabbs Bay is located on the eastern side of the lower SJE and is a relatively sheltered embayment, open towards the south to Galveston Bay. C-20 in Tabbs Bay had a 22.25 cm thick Harvey deposit (Fig. 7) and a HgT concentration of 30 ng g^{-1}, the same concentration found in Clear Lake, above Buffalo Bayou (Fig. 4B). The thick deposit likely results from its sheltered location and its very low HgT concentration suggests either that the deposit is largely made up of sediment from the San Jacinto River or from sediment which settled from the flood water derived from the latter half of the flood from Buffalo Bayou when the floodwaters and sediment were derived from the upper Buffalo Bayou basin (Fig. 3).

Hill (2020) used the distribution of two species of benthic foraminifera, *Ammonia beccari* and *Miliamina fusca*, to determine the provenance of sediment within the Harvey flood layer in the SJE and Galveston Bay. *Ammonia beccari* tolerates a wide range of salinity (5 to 35 psu) making it an excellent indicator of brackish conditions (Boonstra et al., 2015; Dissarda et al., 2010; Melis and Covelli, 2013). *Miliamina fusca* typically denotes freshwater and a tolerance to polluted sediment (Eichler et al., 2004; Eichler et al., 2015). Hill (2020) found a moderate abundance of *Ammonia beccari* in the region from Bear/Clear Lake to Tabbs Bay and a high abundance in upper Galveston Bay. In contrast, Hill (2020), overall, found relatively low abundances of *Miliamina fusca* throughout the bay, but found the highest abundances, by a factor of eight in Tabbs Bay and upper Galveston Bay, just below Morgan Point and very low abundances above Tabbs Bay. The higher abundances of *Miliamina fusca* in Tabbs Bay to lower Galveston Bay indicate that the sediment in this area was likely sourced from freshwater source areas, such as those found within the upper drainage basin of Buffalo Bayou and the San Jacinto River. The low abundance of *Miliamina* and moderate abundances of *Ammonia beccari* for the sediment above Tabbs Bay indicate sediment derived from the brackish water perhaps mixed with terrestrial sources.

Fig. 10 summarizes the observations and findings of the sources and dispersal of sediment and Hg in BB, the SJE, and Galveston Bay. The Hg data, taken together with the textural analyses of sediment and the foraminifera data shows that the Harvey flood deposits found in Burnet and Scott Bay were likely sourced from the lower Buffalo Bayou, where salinities are low but still brackish and San Jacinto River upstream of Burnet Bay. The high integrated HgT concentrations suggest that the source area is both Patrick Bayou and the proximal adjoining section of BB (shown in yellow in Fig. 10) and that the Hg load was primarily delivered during the first phase of the flood. The flood layer found in the lower SJE, including Tabbs Bay as well as upper Galveston Bay (brown layer), suggests an upper drainage basin source and was likely delivered primarily during the post-peak discharge (second phase) of the flood, during the release of water from the Addicks and Barker Reservoirs.

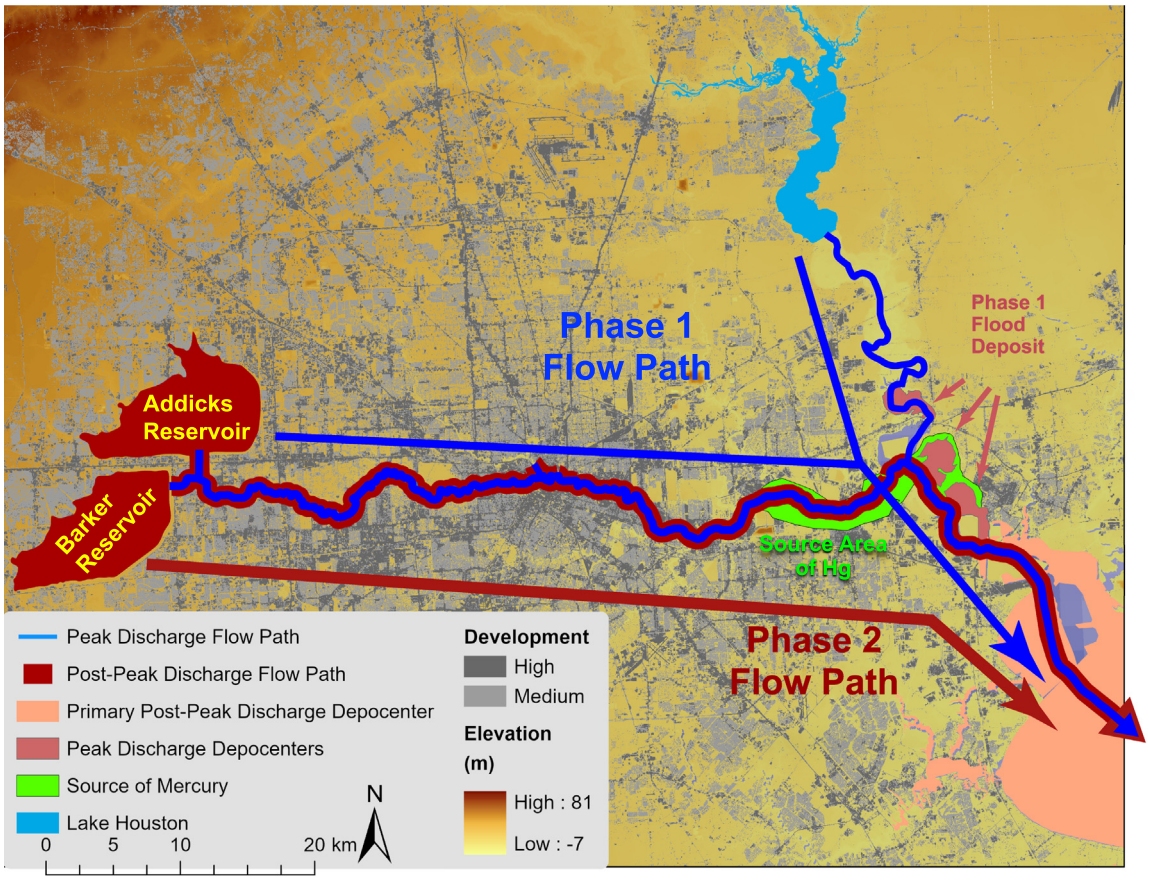

Fig. 10. Conceptual map showing sources and sinks of Hurricane Harvey derived sediment and Hg. During peak discharge, floodwaters (shown in blue) scoured Hg-enriched sediment from lower Buffalo Bayou (BB) and the San Jacinto Estuary (SJE) and sourced a thick deposit of Hg-enriched sediment in Burnet and Scott Bay south of the mouth of BB (shown in red). Additionally, during peak discharge, floodwaters (shown in blue) scoured the SJE, leaving a thick deposit in SJE north of BB. Post peak discharge flooding, including the prolonged release of floodwaters from the Addicks and Barker Reservoirs resulted in the prolonged (44 days) delivery of floodwaters (shown in orange) and basin derived sediment to both the SJE and Galveston Bay (shown in brown).

4.4. HgT, methyl mercury, and enhanced bioavailability

In this study, only HgT was measured, however in marine environments, Hg bioaccumulates as methyl mercury, which is a potent neurotoxin that is among the most widespread contaminants affecting US aquatic ecosystems (Brumbaugh et al., 2001). The anoxic conditions found within estuarine sediment, specifically, under iron, sulfate, methanogenic conditions are where methylmercury is formed (Compeau and Bartha, 1985; Warner et al., 2003; Mason et al., 2006) and more recently it has been found that under these conditions, methylating bacteria are responsible for the rate of methylmercury production and thus bioaccumulation in marine foodwebs (Schartup et al., 2014).

Within the Trinity Bay portion of Galveston Bay, Dellapenna et al. (2006) found the sulfide Redox Potential Discontinuity (RPD) to typically exist within the upper 1–2 cm of the seabed. All of the sediment cores collected in the SJE pre-Harvey and the portions of the post-Harvey cores below the Harvey layer each consisted of black estuarine mud consistent with anoxic sediment. It is reasonable to assume that the RPD resides within the upper few centimeters of the SJE seabed, at least where the substrate is mud dominated, which is generally the case for the areas investigated in this study. This would suggest that nearly the entire sediment column in the SJE is within the zone where methylating bacteria are most active and that the sediment and their porewaters are enriched in methyl mercury proportional to its enrichment in HgT. Consequently, the erosion of these sediments releases elevated amounts of methyl mercury, enhancing its ability to bioaccumulate in the marine food web.

4.5. Potential impacts of the Harvey Storm deposit to the benthic community

In addition to the remobilization, transport, and deposition of legacy contaminants, the massive erosion and deposition of the seabed likely had other impacts on the ecosystem, especially the benthos. The erosion of up to 48 cm of seabed in the SJE is comparable to that which was found in the York River estuary by Dellapenna et al. (1998, 2001, 2003). Schaffner et al. (2001) reported that nearly 50 cm of excavation of sediment in the York River resulted in a loss of all macrobenthic organisms and much of the microbenthic community. Episodic deposition of a thick column of sediment also has a detrimental impact both to the abundance and diversity of benthic communities (Miller et al., 2002; Chou et al., 2004; Naser, 2011).

Thrush et al. (2004) summarized, based on the previous field and laboratory studies, that a critical threshold of episodic deposition of 2 cm in an estuary will quickly create anaerobic conditions within the seabed, resulting in the death of the resident faunal community. The benthic and pelagic coupling within an estuary is central to the nutrient cycling and overall productivity of the system, and an interruption of this coupling resulting from elevated sedimentation rates can have dramatic impacts on the entire ecosystem (Eyre and Ferguson, 2006). Within the lower SJE, there was on average, 22 cm of deposition of new sediment. This suggests the potential for a devastating interruption of the benthic-pelagic coupling of the bay and a significant interruption to the nutrient cycling, at least until the benthic community can ultimately recover. Considering that average sedimentation rates were

already elevated to around 1.5 cm y^{-1} in this system due to elevated land subsidence (Al Mukaimi et al., 2018a), near the 2 cm episodic deposition critical threshold mentioned above (Thrush et al., 2004), it is likely that the benthic community was already stressed. Deposition of 22 cm of sediment in a regime where the sedimentation rate approaches this critical threshold may result in a recovery of the benthos may be much slower than would normally be expected if average sedimentation rates were much lower. It should also be noted that the recovering benthic community will be exposed to elevated levels of a variety of contaminants, including Hg, further exacerbating the situation.

5. Conclusions

The SJE and Buffalo Bayou combined, drain both metropolitan Houston and the Houston Petrochemical complex. Groundwater withdrawal to support both the growing population of Houston as well as the massive petrochemical complex has resulted in 3 m of land subsidence. The accommodation space created this subsidence resulted in the accumulation and archiving of more than 2 m of sediment which contained elevated concentrations of particle-bound and porewater contaminants, including Hg. Industrial wastewater outfalls within Patrick Bayou, located along lower Buffalo Bayou, are the primary source of Hg for the sediments within lower Buffalo Bayou and the SJE, as well as Galveston Bay. Cores from Patrick Bayou reveal HgT concentrations as high as 51,270 ng g^{-1} at a depth of 19.5 cm, which is over 1000 times background concentrations and is the highest concentration found anywhere within Galveston Bay, by a factor of 20.

The extreme rainfall from Harvey delivered 14×10^9 m^3 of freshwater to Galveston Bay and produced record flooding of the Houston bayous and waterways, most of which flowed through Buffalo Bayou and the SJE. The flooding of Buffalo Bayou and the SJE during Harvey can be divided into two phases, the first phase occurred during the peak discharge and the second half occurred during the falling limb of the hydrograph. The entire flood event for the San Jacinto River and other tributaries occurred over a 12–16 day period, however, due to the release of floodwaters from the Barker and Addicks Reservoir, the flood lasted for a total of 53 days for Buffalo Bayou.

Detailed analyses of sediment cores collected within both Patrick Bayou and Scott Bay reveal extensive erosion during the rising flood waters and that the transport of sediment was modulated by the two phases of the flood. Within Scott Bay, Harvey the rising flood waters during the first phase of the flood eroded 48 cm of the sediment, exporting of 16.42×10^6 tons of sediment which contained 2.0 tons of HgT to Galveston Bay. Within Patrick Bayou, it is estimated that 130 cm of sediment was eroded, exporting 1.43×10^5 tons of sediment and 1.43 tons of HgT downstream into the SJE and Galveston Bay. Additionally, overall, in Scott Bay, a 22 cm thick flood layer was deposited and within the SJE, Harvey deposited 7.73×10^6 tons of sediment and 0.96 tons of HgT within the SJE. The basal layer contains shell lag gravel, was likely sourced from the upper SJE and from the lower reach of Buffalo Bayou, during the first phase of the flood. The upper layer is mud dominated, represents the suspended load and was deposited during the second phase of the flood.

Within Patrick Bayou, the basal layer contains extremely elevated HgT concentrations (as high as 24,011 ng g^{-1}) and lower sand content, which indicate that it formed during the first phase of the flood and was sourced primarily from eroded local sediment within the bayou and its drainage basin. The upper layer of the Patrick Bayou Harvey deposit contains a higher sand content and lower HgT. This indicates that this deposit was derived from a combination of upper drainage basin sands derived from the scouring of the river bed mixed with sediment from lower Buffalo Bayou, which contain Hg originally derived primarily from Patrick Bayou.

The Harvey deposit was found to be thickest within the upper SJE above the confluence with Buffalo Bayou within Clear and Bear Lake Bays and just below the confluence of Buffalo Bayou, within Burnett, Crystal, and Scott Bays and thinned southward towards Morgan Point and within the upper Galveston Bay. The Harvey deposit HgT concentrations were found highest within lower Buffalo Bayou and within the same section of the SJE where the Harvey deposit is thickest downstream of the confluence of Buffalo Bayou. The thicker Harvey deposits upstream of the confluence contained background levels of HgT, suggesting that there are no significant sources of Hg coming from upstream of the confluence with Buffalo Bayou. When pre- and post-Harvey HgT distributions are compared, the greatest enrichment is within Burnett Bay at the mouth of Buffalo Bayou. Analyses of foraminifera from cores Scotts Bay as well as from the Harvey deposit from around the SJE indicate the Harvey deposit found within the lowermost SJE and upper reaches of Galveston Bay are enriched in freshwater foraminifera, suggesting that the Harvey deposit found in this area was sourced from the upper drainage basin of Buffalo Bayou. In contrast, the foraminifera found within the Harvey deposit found within Scott, Crystal, and Burnett and surrounding areas were dominated by brackish species. The combined foraminifera HgT distributions strongly suggest that during the initial phase of the flood, sediment from the lower portion of Buffalo Bayou, potentially including Patrick Bayou, were flushed into the semi-sheltered bays of Burnett, Crystal and Scott Bays where they settled proximal to the mouth of Buffalo Bayou, where much of this material was sources during waning half of the first phase of the flood, with a significant component of the deposit comprising bedload material. The second phase of the storm primarily delivered suspended sediment, which was able to be more broadly distributed, hence its greater representation within the lower section of the SJE and upper Galveston Bay.

Elevated land subsidence is a feature of many of the world's urbanized estuaries and deltas and provides a mechanism for the accumulation and archiving of elevated concentration of both particle-bound and porewater contaminants. The conventional wisdom prior to this study was that deeply buried legacy contaminants in estuaries are not of concern because their deeper burial makes them not susceptible to erosion. However, this study shows that intense flooding within estuaries can erode decimeters of sediment, and is in fact, capable of eroding deeply buried legacy contaminants and dispersing tons of these contaminants around the estuarine system.

Within the SJE and Galveston Bay, as well as many of the world's estuaries, Hg is a significant contaminant. Although this study only investigated HgT, Hg bioaccumulates as methyl mercury. Methyl mercury forms within the anoxic conditions found a few centimeters below the surface within estuarine muds. In the context of Hg, it also mobilizes the most toxic forms of Hg, enabling it to be much more bioavailable and enhancing its ability to bioaccumulate in the marine food web. When we consider Harvey and the legacy contaminants archived with the SJE, within Scott Bay, the layer with the highest concentration of HgT was not eroded, but this layer was likely eroded in other parts of the SJE. However, within Scott Bay, this layer is now at least 20 cm shallower than before the storm, making it much more vulnerable to erosion during the next large flood event. When we consider that the frequency of slow-moving tropical cyclones capable of delivering devastating rainfall is increasing, then we can expect an increase in the frequency of extreme flood events that are capable of excavating deeply buried legacy contaminants from the archive of sediment within urbanized estuaries. Consequently, what happened during Harvey is a harbinger of what is to come both for Galveston Bay as well as other urbanized estuaries and deltas around the world.

CRediT authorship contribution statement

Timothy M. Dellapenna: Writing - original draft, Investigation, Formal analysis, Data curation, Conceptualization, Visualization, Methodology, Validation, Resources, Supervision, Writing - review & editing. **Christena Hoelscher:** Visualization, Software. **Lisa Hill:** Investigation, Visualization, Methodology. **Mohammad E. Al Mukaimi:** Writing -

review & editing. **Anthony Knap:** Funding acquisition, Resources, Writing - review & editing.

Declaration of competing interest

The authors declare that they have no known competing financial interests or personal relationships that could have appeared to influence the work reported in this paper.

Acknowledgements

We would like to acknowledge the many undergraduate and graduate students who have helped with both the field and lab phases of this work, including M. Bell, O. Cavazos, J. Lewis, N. Wellbrock, A. Bland, and L. Critides. This work was partially supported by the National Institute of Environmental Health Sciences of the National Institutes of Health under Award P42 ES027704 and by the Texas General Land Office and the National Oceanic and Atmospheric Administration (NOAA) through the Texas Coastal Management Program under Award 19-040-000-B074.

References

Al Mukaimi, M.E., Dellapenna, T.M., Williams, J.R., 2018a. Enhanced land subsidence in Galveston Bay, Texas: interaction between sediment accumulation rates and relative sea level rise. Estuar. Coast. Shelf Sci. 207, 183–193. https://doi.org/10.1016/j.ecss.2018.03.023.

Al Mukaimi, M.E., Kaiser, K., Williams, J.R., Dellapenna, T.M., Louchouarn, P., Santschi, P.H., 2018b. Centennial record of anthropogenic impacts in Galveston Bay: evidence from trace metals (Hg, Pb, Ni, Zn) and lignin oxidation products. Environ. Pollut. 237, 887–899. https://doi.org/10.1016/j.envpol.2018.01.027.

Armstrong, N.E., 1982. Responses of Texas estuaries to freshwater inflows. Estuarine Comparisons. Academic Press, pp. 103–120 https://doi.org/10.1016/B978-0-12-404070-0.50013-2.

Ayuso, R.A., Foley, N.K., Seal II, R.R., Bove, M., Civitillo, D., Cosenza, A., Grezzi, G., 2013. Lead isotope evidence for metal dispersal at the Callahan Cu–Zn–Pb mine: Goose Pond tidal estuary, Maine, USA. J. Geochem. Explor. 126, 1–22. https://doi.org/10.1016/j.gexplo.2012.12.013.

Bank, M.S., 2012. Mercury in the Environment: Pattern and Process. Univ. of California Press.

Bera, G., Camargo, K., Sericano, J.L., Liu, Y., Sweet, S.T., Horney, J., Jun, M., Chiu, W., Rusyn, I., Wade, T.L., Knap, A.H., 2019. Baseline data for distribution of contaminants by natural disasters: results from a residential Houston neighborhood during Hurricane Harvey flooding. Heliyon 5 (11). https://doi.org/10.1016/j.heliyon.2019.e02860 (p.e 02860).

Boonstra, M., Ramos, M., Lammertsma, E., Antoine, P., Hoorn, C., 2015. Marine connections of Amazonia: evidence from foraminifera and dinoflagellate cysts (early to middle Miocene, Colombia/Peru). Palaeogeogr. Palaeoclimatol. Palaeoecol. 417, 176–194. https://doi.org/10.1016/j.palaeo.2014.10.032.

Brumbaugh, W.G., Krabbenhoft, D.P., Helsel, D.R., Wiener, J.G., Echols, K.R., 2001. A national pilot study of mercury contamination of aquatic ecosystems along multiple gradients: bioaccumulation in fish. Biological Science Report 9. https://semspub.epa.gov/work/01/466771.pdf.

Buchman, M., 2008. NOAA screening quick reference tables, NOAA OR&R report 08-1. Office of Response and Restoration Division, National Oceanic and Atmospheric Administration, Seattle , p. 34. https://repository.library.noaa.gov/view/noaa/9327.

Carlin, J.A., Lee, G., Dellapenna, T.M., Laverty, P., 2016. Sediment resuspension by wind, waves, and currents during meteorological frontal passages in a micro-tidal lagoon. Estuar. Coast. Shelf Sci. 172, 24–33. https://doi.org/10.1016/j.ecss.2016.01.029.

Cave, R.R., Andrews, J.E., Jickells, T., Coombes, E.G., 2005. A review of sediment contamination by trace metals in the Humber catchment and estuary, and the implications for future estuary water quality. Estuar. Coast. Shelf Sci. 62 (3), 547–557. https://doi.org/10.1016/j.ecss.2004.09.017.

Chambers, M., Mitchell, A., Fine, A., Mulder, K., Rainville, L., Hackett, D., Smith, D., Dijoseph, P., Kress, M., Mitchell, K.N., Tujague, A., 2018. Port performance freight statistics program: annual report to congress 2017. [Supporting Datasets]. https://www.bts.gov/browse-statistical-products-and-data/port-performance/port-performance-freight-statistics-program.

Chou, L., Yu, J., Loh, T., 2004. Impacts of sedimentation on soft-bottom benthic communities in the southern islands of Singapore. Hydrobiologia 515 (1–3), 91–106. https://doi.org/10.1023/B:HYDR.0000027321.23230.2f.

Ciszewski, D., Grygar, T.M., 2016. A review of flood-related storage and remobilization of heavy metal pollutants in river systems. Water Air Soil Pollut. 227 (7), 239. https://doi.org/10.1007/s11270-016-2934-8.

Compeau, G., Bartha, R., 1985. Sulfate-reducing bacteria: principal methylators of mercury in anoxic estuarine sediment. Appl.Environ.Microbiol. 50 (2), 498–502.

Coplin, L.S., Galloway, D., 1999. Houston-Galveston, Texas. Land Subsidence in the United States: US Geological Survey Circular. vol. 1182 , pp. 35–48. https://www.researchgate.net/profile/Devin_Galloway/publication/284221420_Houston-Galveston_Texas_Managing_coastal_subsidence/links/565867e408ae4988a7b7454f.pdf.

Cutshall, N.H., Larsen, I.L., Nichols, M.M., 1981. Man-made radionuclides confirm rapid burial of kepone in James River sediments. Science 213 (4506), 440–442. https://doi.org/10.1126/science.213.4506.440.

de Souza Machado, A.A., Spencer, K., Kloas, W., Toffolon, M., Zarfl, C., 2016. Metal fate and effects in estuaries: a review and conceptual model for better understanding of toxicity. Sci. Total Environ. 541, 268–281. https://doi.org/10.1016/j.scitotenv.2015.09.045.

Dellapenna, T., Kuehl, S., Schaffner, L., 1998. Sea-bed mixing and particle residence times in biologically and physically dominated estuarine systems: a comparison of lower Chesapeake Bay and the York River subestuary. Estuar. Coast. Shelf Sci. 46 (6), 777–795. https://doi.org/10.1006/ecss.1997.0316.

Dellapenna, T.M., Kuehl, S.A., Pitts, L., 2001. Transient, longitudinal, sedimentary furrows in the York River subestuary, Chesapeake Bay: furrow evolution and effects on seabed mixing and sediment transport. Estuaries 24, 215–227. www.jstor.org/stable/1352946.

Dellapenna, T.M., Kuehl, S.A., Schaffner, L.C., 2003. Ephemeral deposition, seabed mixing and fine-scale strata formation in the York River estuary, Chesapeake Bay. Estuar. Coast. Shelf Sci. 58 (3), 621–643. https://doi.org/10.2307/1352946.

Dellapenna, T.M., Allison, M.A., Gill, G.A., Lehman, R.D., Warnken, K.W., 2006. The impact of shrimp trawling and associated sediment resuspension in mud dominated, shallow estuaries. Estuar. Coast. Shelf Sci. 69 (3–4), 519–530. https://doi.org/10.1016/j.ecss.2006.04.024.

Di Leonardo, R., Tranchida, G., Bellanca, A., Neri, R., Angelone, M., Mazzola, S., 2006. Mercury levels in sediments of Central Mediterranean Sea: a 150 year record from box-cores recovered in the Strait of Sicily. Chemosphere 65 (11), 2366–2376. https://doi.org/10.1016/j.chemosphere.2006.04.076.

Dissarda, D., Nehrke, G., Reichart, G.J., Bijma, J., 2010. The impact of salinity on the Mg/Ca and Sr/Ca ratio in the benthic foraminifera *ammonia tepida*: results from culture experiments. Geochim. Cosmochim. Acta 74 (3), 928–940. https://doi.org/10.1016/j.gca.2009.10.040.

Du, J., Park, K., Dellapenna, T.M., Clay, J.M., 2019a. Dramatic hydrodynamic and sedimentary responses in Galveston Bay and adjacent inner shelf to Hurricane Harvey. Sci. Total Environ. 653, 554–564. https://doi.org/10.1016/j.scitotenv.2018.10.403.

Du, J., Park, K., Dellapenna, T.M., Clay, J.M., 2019b. Corrigendum to "Dramatic hydrodynamic and sedimentary responses in Galveston Bay and adjacent inner shelf to Hurricane Harvey" [Sci. Total Environ. 653 (2019b), 554–564]. Sci. Total Environ. 697, 134219. https://doi.org/10.1016/j.scitotenv.2019.134219.

Eichler, P.P.B., Castelão, G.P., Pimenta, F.M., Eichler, B.B., De Miranda, L.B., Rodrigues, A.R., Pereira, E.R., 2004. Foraminifera and thecamoebians as indicator of hydrodynamic process in a choked coastal lagoon, Laguna estuarine system, SC, Brazil. J. Coast. Res. 39, 1144–1148.

Eichler, P.P.B., Eichler, B.B., Vital, H., 2015. Marine pollution-environmental indicators in marine meiofauna from Brazil. Environmental Indicators, 545–560 https://doi.org/10.1007/978-94-017-9499-2_32 (Springer).

EPA, 1998. Method 7473: Mercury in Solids and Solutions by Thermal Decomposition Amalgamation and Atomic Absorption Spectrophotometry, EPA SW-846. USEPA Office of Research and Development Environmental Monitoring Systems Labratory, Cincinnati.

Eyre, B.D., Ferguson, A.J., 2006. Impact of a flood event on benthic and pelagic coupling in a sub-tropical east Australian estuary (Brunswick). Estuar. Coast. Shelf Sci. 66 (1–2), 111–122. https://doi.org/10.1016/j.ecss.2005.08.008.

He, J., Soden, B.J., 2015. Anthropogenic weakening of the tropical circulation: the relative roles of direct CO2 forcing and sea surface temperature change. J. Clim. 28 (22), 8728–8742. https://doi.org/10.1175/JCLI-D-15-0205.1.

He, J., Winton, M., Vecchi, G., Jia, L., Rugenstein, M., 2017. Transient climate sensitivity depends on base climate ocean circulation. J. Clim. 30 (4), 1493–1504. https://doi.org/10.1175/JCLI-D-16-0581.1.

Held, I.M., Soden, B.J., 2006. Robust responses of the hydrological cycle to global warming. J. Clim. 19 (21), 5686–5699. https://doi.org/10.1175/JCLI3799.1.

HGAC (Houston-Galveston Area Council), 2012. Patrick Bayou Site Status Report Patrick Bayou Superfund Site. http://www.h-gac.com/watershed-based-plans/documents/hsc-ugb/hsc_04-04-2012_Patrick-Bayou-Superfund-Site.pdf.

HGSD, 2008. Houston Galveston Subsidence District- Subsidence: 1906–2000. Available at. http://www.subsidence.org/Assets/PDFDocuments/.

HGSD, 2013. Subsidence and groundwater regulation FAQ's. Available at. http://hgsubsidence.org/frequently-asked-questions/subsidence-groundwater-regulation-faqs/.

Hill, L., 2020. Environmental and Anthropogenic Influences during the 20th Century in Scott Bay. San Jacinto Estuary, Houston, Texas (Unpublished manuscript).

Jelgersma, S., 1996. Land subsidence in coastal lowlands. Sea-Level Rise and Coastal Subsidence. Springer, Dordrecht, pp. 47–62 https://doi.org/10.1007/978-94-015-8719-8_3.

Kennish, M.J., 2002. Environmental threats and environmental future of estuaries. Environ. Conserv. 29 (1), 78–107. https://doi.org/10.1017/S0376892902000061.

Knap, A.H., Rusyn, I., 2016. Environmental exposures due to natural disasters. Rev. Environ. Health 31 (1), 89–92.

Kossin, J.P., 2018. A global slowdown of tropical-cyclone translation speed. Nature 558 (7708), 104–107. https://doi.org/10.1038/s41586-018-0158-3.

Liu, G., Cai, Y., O'Driscoll, N., 2011. Environmental Chemistry and Toxicology of Mercury. John Wiley & Sons.

Macklin, M.G., Hudson-Edwards, K.A., Dawson, E.J., 1997. The significance of pollution from historic metal mining in the Pennine orefields on river sediment contaminant fluxes to the North Sea. Sci. Total Environ. 194, 391–397. https://doi.org/10.1016/S0048-9697(96)05378-8.

Mann, M.E., Rahmstorf, S., Kornhuber, K., Steinman, B.A., Miller, S.K., Coumou, D., 2017. Influence of anthropogenic climate change on planetary wave resonance and extreme weather events. Sci. Rep. 7, 45242. https://doi.org/10.1126/sciadv.aat3272.

Mason, R.P., Kim, E., Cornwell, J., Heyes, D., 2006. An examination of the factors influencing the flux of mercury, methylmercury and other constituents from estuarine sediment. Mar. Chem. 102 (1–2), 96–110. https://doi.org/10.1016/j.marchem.2005.09.021.

Melis, R., Covelli, S., 2013. Distribution and morphological abnormalities of recent foraminifera in the Marano and Grado lagoon (North Adriatic Sea, Italy). Mediterr. Mar. Sci. 14 (2), 432–450. https://doi.org/10.12681/mms.351.

Miller, D.C., Muir, C.L., Hauser, O.A., 2002. Detrimental effects of sedimentation on marine benthos: what can be learned from natural processes and rates? Ecol. Eng. 19 (3), 211–232. https://doi.org/10.1016/S0925-8574(02)00081-2.

Morse, J.W., Presley, B.J., Taylor, R.J., Benoit, G., Santschi, P., 1993. Trace metal chemistry of Galveston Bay: water, sediments and biota. Mar. Environ. Res. 36 (1), 1–37. https://doi.org/10.1016/0141-1136(93)90087-G.

Naser, H.A., 2011. Effects of reclamation on macrobenthic assemblages in the coastline of the Arabian Gulf: a microcosm experimental approach. Mar. Pollut. Bull. 62 (3), 520–524. https://doi.org/10.1016/j.marpolbul.2010.11.032.

NOAA- National Oceanic and Atmospheric Administration, Office for Coastal Management, 2016. 2016 C-CAP Regional Land Cover. Coastal Change Analysis Program (C-CAP) Regional Land Cover. NOAA Office for Coastal Management, Charleston, SC. Accessed June 2020 at. www.coast.noaa.gov/htdata/raster1/landcover/bulkdownload/30m_lc/.

NOAA- National Oceanic and Atmospheric Administration, 2017. NOAA National Centers for Environmental Information, State of the Climate: National Climate Report for Annual 2017. published online January 2018, retrieved on June 11, 2020 from. https://www.ncdc.noaa.gov/sotc/national/201713.

Olsen, C.R., Larsen, I.L., Mulholland, P.J., Von Damm, K.L., Grebmeier, J.M., Schaffner, L.C., Diaz, R.J., Nichols, M.M., 1993. The concept of a equilibrium surface applied to particle sources and contaminant distributions in estuarine sediments. Estuaries 16 (3), 683–696. https://doi.org/10.2307/1352805.

O'Shea, F.T., Cundy, A.B., Spencer, K.L., 2018. The contaminant legacy from historic coastal landfills and their potential as sources of diffuse pollution. Mar. Pollut. Bull. 128, 446–455. https://doi.org/10.1016/j.marpolbul.2017.12.047.

Plumlee, G.S., Morman, S.A., Meeker, G.P., Hoefen, T.M., Hageman, P.L., Wolf, R.E., 2013. The environmental and medical geochemistry of potentially hazardous materials produced by disasters. Treatise on Geochemistry 11, 257–304. http://www.sciiencediirect.com/sciience/artiiclle/piii/B9780080959757009074.

Ren, W., Duan, L., Zhu, Z., Du, W., An, Z., Xu, L., Zhang, C., Zhuo, Y., Chen, C., 2014. Mercury transformation and distribution across a polyvinyl chloride (PVC) production line in China. Environmental Science & Technology 48 (4), 2321–2327. https://doi.org/10.1021/es404147c.

Rodriguez, A.B., Anderson, J.B., Simms, A.R., 2005. Terrace inundation as an autocyclic mechanism for parasequence formation: Galveston Estuary, Texas, U.S.A. J. Sediment. Res. 75, 608–620. https://doi.org/10.2110/jsr.2005.050.

Rodriguez-Iruretagoiena, A., de Vallejuelo, S.F.O., de Diego, A., de Leão, F.B., de Medeiros, D., Oliveira, M.L., Tafarel, S.R., Arana, G., Madariaga, J.M., Silva, L.F., 2016. The mobilization of hazardous elements after a tropical storm event in a polluted estuary. Sci. Total Environ. 565, 721–729. https://doi.org/10.1016/j.scitotenv.2016.05.024.

Santschi, P.H., Presley, B.J., Wade, T.L., Garcia-Romero, B., Baskaran, M., 2001. Historical contamination of PAHs, PCBs, DDTs, and heavy metals in Mississippi River Delta, Galveston Bay and Tampa Bay sediment cores. Mar. Environ. Res. 52 (1), 51–79. https://doi.org/10.1016/S0141-1136(00)00260-9.

Schaffner, L.C., Dellapenna, T.M., Hinchey, E.K., Friedrichs, C.T., Neubauer, M.T., Smith, M.E., Kuehl, S.A., 2001. Physical energy regimes, seabed dynamics and organism-sediment interactions along an estuarine gradient. Organism-Sediment Interactions 159–179.

Schartup, A.T., Balcom, P.H., Mason, R.P., 2014. Sediment-porewater partitioning, total sulfur, and methylmercury production in estuaries. Environmental Science & Technology 48 (2), 954–960. https://doi.org/10.1021/es403030d.

Schoellhamer, D.H., Mumley, T.E., Leatherbarrow, J.E., 2007. Suspended sediment and sediment-associated contaminants in San Francisco Bay. Environ. Res. 105 (1), 119–131. https://doi.org/10.1016/j.envres.2007.02.002.

Solis, R.S., Powell, G., 1999. Hydrography, residence times, and physical processes. Biogeochemistry of Gulf of Mexico Estuaries. John Wiley, New York, pp. 29–61.

Swales, A., Williamson, R.B., Van Dam, L.F., Stroud, M.J., McGlone, M.S., 2002. Reconstruction of urban stormwater contamination of an estuary using catchment history and sediment profile dating. Estuaries 25 (1), 43–56. https://doi.org/10.1007/BF02696048.

Syvitski, J.P., Kettner, A.J., Overeem, I., Hutton, E.W., Hannon, M.T., Brakenridge, G.R., Day, J., Vörösmarty, C., Saito, Y., Giosan, L., Nicholls, R.J., 2009. Sinking deltas due to human activities. Nat. Geosci. 2 (10), 681–686. https://doi.org/10.1038/ngeo629.

Tessler, Z.D., Vörösmarty, C.J., Grossberg, M., Gladkova, I., Aizenman, H., Syvitski, J.P.M., Foufoula-Georgiou, E., 2015. Profiling risk and sustainability in coastal deltas of the world. Science 349 (6248), 638–643. https://doi.org/10.1126/science.aab3574.

Thrush, S., Hewitt, J., Cummings, V., Ellis, J., Hatton, C., Lohrer, A., Norkko, A., 2004. Muddy waters: elevating sediment input to coastal and estuarine habitats. Front. Ecol. Environ. 2 (6), 299–306. https://doi.org/10.1890/1540-9295(2004)002[0299:MWESIT]2.0.CO;2.

TNRIS - Texas Natural Resources Information System, 2014. Texas Rivers, Streams, and Waterbodies, 2014-02-01. Retrieved on 2020-06-16 from. https://tnris.org.

TPWD - Texas Parks and Wildlife Department, 2013. GIS Maps and Spatial Data: Coastal Bathymetry, 2013-02-01. Retrieved on 2020-06-15 from. https://tpwd.texas.gov/gis/gis-main.

Turner, J.N., Brewer, P.A., Macklin, M.G., 2008. Fluvial-controlled metal and As mobilisation, dispersal and storage in the Río Guadiamar, SW Spain and its implications for long-term contaminant fluxes to the Doñana wetlands. Sci. Total Environ. 394 (1), 144–161. https://doi.org/10.1016/j.scitotenv.2007.12.021.

Uncles, R.J., Stephens, J.A., Woodrow, T.Y., 1988. Seasonal cycling of estuarine sediment and contaminant transport. Estuaries 11 (2), 108. https://doi.org/10.2307/1351998.

US EPA -United States Environmental Protection Agency, 2017. Patrick Bayou Site Profile. Retrieved on 2020- 03-20 from. https://cumulis.epa.gov/supercpad/SiteProfiles/index.cfm?fuseaction=second.Cleanup&id=0605329#bkground.

USGS - United States Geological Survey, 2013. National Elevation Dataset, 2013-01-01. Retrieved on 2020-06-15 from. https://catalog.data.gov/dataset/usgs-national-elevation-dataset-ned.

Vallette, J., 2018. Chlorine and building materials: a global inventory of production technologies, market, and pollution, phase 1: Africa, the Americas and Europe. HBN Know Better Healthy Building Network, Washington D.Chttps://healthybuilding.net/reports/18-chlorine-building-materials-project-phase-1-africa-the-americas-and-europe.

Vecchi, G.A., Soden, B.J., 2007. Global warming and the weakening of the tropical circulation. J. Clim. 20 (17), 4316–4340. https://doi.org/10.1175/JCLI4258.1.

Vecchi, G.A., Soden, B.J., Wittenberg, A.T., Held, I.M., Leetmaa, A., Harrison, M.J., 2006. Weakening of tropical Pacific atmospheric circulation due to anthropogenic forcing. Nature 441 (7089), 73–76. https://doi.org/10.1038/nature04744.

Walsh, K.J., McBride, J.L., Klotzbach, P.J., Balachandran, S., Camargo, S.J., Holland, G., Knutson, T.R., Kossin, J.P., Lee, T.C., Sobel, A., Sugi, M., 2016. Tropical cyclones and climate change. Wiley Interdiscip. Rev. Clim. Chang. 7 (1), 65–89. https://doi.org/10.1002/wcc.371.

Ward, G.H., 1980. Hydrography and circulation processes of gulf estuaries. Estuarine and Wetland Processes. Springer, pp. 183–215 https://doi.org/10.1007/978-1-4757-5177-2_7.

Warner, K.A., Roden, E.E., Bonzongo, J., 2003. Microbial mercury transformation in anoxic freshwater sediments under iron-reducing and other electron-accepting conditions. Environmental Science & Technology 37 (10), 2159–2165. https://doi.org/10.1021/es0262939.

Williams, J., Dellapenna, T., Louchouarn, P., Lee, G., 2015. Historical reconstruction of anthropogenic mercury input from sedimentary records: Yeongsan estuary, South Korea. Estuar. Coast. Shelf Sci. 167, 436–446. https://doi.org/10.1016/j.ecss.2015.10.021.